Spring 5-1-2021

A triple oxygen isotope analysis of altered oceanic crust and its buffering effect on the steady state oxygen isotope composition of seawater

Jesse P. McGunnigle

Jesse Patrick McGunnigle
Candidate

Earth and Planetary Sciences
Department

This thesis is approved, and it is acceptable in quality and form for publication:

Approved by the Thesis Committee:

Dr. Zachary Sharp, Chairperson

Dr. Adrian Brearley

Dr. Brandon Schmandt

A TRIPLE OXYGEN ISOTOPE ANALYSIS OF ALTERED OCEANIC CRUST AND ITS BUFFERING EFFECT ON THE STEADY STATE OXYGEN ISOTOPE COMPOSITION OF SEAWATER

by

JESSE PATRICK MCGUNNIGLE

A.A., LIBERAL ARTS AND SCIENCES, SUFFOLK COUNTY COMMUNITY COLLEGE, 2016
B.S., GEOLOGY, UNIVERSITY OF PITTSBURGH, 2019

THESIS

Submitted in Partial Fulfillment of the
Requirements for the Degree of

Master of Science
Earth and Planetary Sciences

The University of New Mexico
Albuquerque, New Mexico

May, 2021

ACKNOWLEDGEMENTS:

I would like to express my sincerest thanks to my committee chair, Dr. Zachary Sharp, for allowing me the opportunity to spend my time in graduate school on a project that keenly interested me. Zach's enthusiasm for the field of stable isotope geochemistry is contagious and instilled in me a desire to address a contentious issue that has plagued the field since its genesis. His input on this project was indispensable and enabled both me and the project to develop and grow in many ways throughout the research process. I would also like to thank the other members of my committee, Dr. Adrian Brearley, and Dr. Brandon Schmandt for their constructive comments and questions during the initial stages of the research.

To the staff of the Center for Stable Isotopes, especially Dr. Viorel Atudorei and Dr. Laura Burkemper, I would like to express my earnest gratitude for keeping the labs running during this challenging past year and enabling me to safely run samples throughout the pandemic. Without their swift and thorough response to UNM safety concerns and state orders, CSI research would have halted for longer than necessary and the submission of this thesis would have been significantly delayed. I would also like to thank Chris Anderson for always offering his engineering skills to make the day to day technical issues of the lab promptly disappear. A special thank you to Erick Cano, Dr. Jordan Wostbrock, and Dr. Karen Ziegler for teaching me how to use the laser, "bombs", O_2 line, mass spectrometers, and software necessary to measure triple oxygen isotopes. The Integrated Ocean Drilling Programming, Dr. Karlis Muehlenbachs, and Dr. David Cole all have my thanks for providing the samples absolutely necessary to make this project happen. Karlis also has my thanks for helping me to better understand his mass balance model, as well as sample preparation techniques for analyzing oceanic crust to help ensure our quality of data. Thank you also to the NSF for funding this work.

Thank you to my fiancée, Meredith, for her perpetual support, editing input, help formatting, and willingness to move across the country so that I can go be a "rock nerd." Thank you to my brother, Zach, for always willingly offering his expertise whenever I ran into a tech-related issue. And finally, thank you to my parents for always supporting me in every endeavor I have undertaken, even the more questionable ones…

A triple oxygen isotope analysis of altered oceanic crust and its buffering effect on the steady state oxygen isotope composition of seawater

by

Jesse Patrick McGunnigle

A.A., Liberal Arts and Sciences, Suffolk County Community College, 2016
B.S., Geology, University of Pittsburgh, 2019
M.S., Earth and Planetary Sciences, University of New Mexico, 2021

ABSTRACT

The secular chemical marine sediment trend showing an increase in $\delta^{18}O$ over geologic time has traditionally been investigated using $\delta^{18}O$ modelling of ancient ocean compositions, ocean surface temperatures, and sample diagenetic alteration. This study presents a triple oxygen isotope mass balance for the oceans using high precision $\delta^{18}O$ and $\Delta'^{17}O$ measurements of altered oceanic crust. The mass balance model predicts an ice-free seawater with $\delta^{18}O$ = -0.29‰ and $\Delta'^{17}O$ = -0.002‰ with steady state reached at approximately (0.5 to 1)×10^9 years. Modifications to the hydrothermal alteration and continental weathering fluxes to examine Archean ocean compositions predict seawater evolution slopes of λ = 0.524 and λ = 0.529, respectively. A model generated seawater of $\delta^{18}O$ = -4.1‰ and $\Delta'^{17}O$ = 0.014‰ predicts previously published Archean chert data precipitated in an ocean with 50 - 60°C surface temperatures and lost primary $\delta^{18}O$ and $\Delta'^{17}O$ signals from diagenetic alteration with low $\delta^{18}O$ fluids.

TABLE OF CONTENTS

LIST OF FIGURES

LIST OF TABLES

1. INTRODUCTION

Oxygen isotope measurements of marine chemical sediments yield lower $\delta^{18}O$ values for ancient sediments compared to complementary modern samples, with an approximately linear trend of increasing $\delta^{18}O$ value with decreasing sample age. This phenomenon appears to have three possible geological explanations: 1) lower $\delta^{18}O$ values for ancient oceans that have increased through time, 2) higher ancient ocean temperatures that have decreased over time, and 3) lowered $\delta^{18}O$ of marine sediments via diagenetic fluid-rock (F/R) interaction. The present oxygen isotope composition of seawater is thought to be buffered by F/R interactions during tectonic processes with a mean $\delta^{17}O$ and $\delta^{18}O$ value approximately equal to 0‰ (Muehlenbachs, 1998).

Lower $\delta^{18}O$ values of ancient seawater have been suggested by Veizer et al. (1999), Wallmann (2001), Kasting et al. (2006), Jaffres et al. (2007), Shields (2007), and would likely indicate temporal variations in the way plate tectonics have operated as well as a 5‰ increase in seawater $\delta^{18}O$ per billion years (Weber, 1965; Perry, 1967; Muehlenbachs, 1976). Alternatively, it has been proposed that distinct ancient weathering processes reflected in the $\delta^{18}O$ values of Archean hydrothermally altered basaltic crust resulted in a higher seawater $\delta^{18}O$ value of 3.3‰ (Johnson and Wing, 2020). Higher ocean temperatures have been proposed in many publications, including Knauth and Epstein (1976), Knauth and Lowe (1978), Karhu and Epstein (1985), and more recently Tartese et al. (2017) and Garcia et al. (2017). If seawater $\delta^{18}O$ has remained constant through time, then the low $\delta^{18}O$ values of ancient sediments would require remarkably high ocean

temperatures hostile to life (Carpenter et al., 1991). Diagenetic alteration can lower the $\delta^{18}O$ of ancient sediments, but the magnitude has been shown to vary by mineral species and in the case of brachiopods, to be a process strongly independent of fossil age, a finding inconsistent with the marine sediment record trend occurring independently of sediment type and species (Banner and Hanson, 1990; Wenzel et al., 2000). Diagenetic alteration requires the interaction of the sediment with a low $\delta^{18}O$ meteoric water at either high or low temperature conditions, or sediment-seawater interaction at high temperatures (Degens and Epstein, 1962).

Expansion of oxygen isotope analyses of chemical marine sediments to include the rare ^{17}O isotope introduces a second mass-dependent fractionation process that can be used to further examine the marine sediment secular trend. (Data are presented in terms of $\delta^{18}O$ and $\Delta'^{17}O$ values – see **Appendix III** for definition). Recent triple oxygen isotope analyses of pristine Archean cherts suggest one of three explanations: 1) the ancient ocean $\delta^{18}O$ and $\Delta'^{17}O$ values were similar to the modern ice-free Earth with higher ocean temperatures ranging from 66 to 76°C (Lowe et al., 2020); 2) Diagenetic alteration with a meteoric fluid lowered the $\delta^{18}O$ and $\Delta'^{17}O$ values of ancient cherts (Liljestrand et al. 2020; Sengupta et al., 2020). Sengupta et al. (2020) propose a diagenetic model with a large range in initial meteoric fluid composition, but not a hot and isotopically light early ocean environment; 3) a high temperature hydrothermal origin. At least some ancient chert deposits have primary quartz that was precipitated at temperatures between 150 and 170°C with contributions from hydrothermal vent fluids (Zakharov et al., 2019). The results do not require a change in the $\delta^{18}O$ value of the ancient ocean.

The variability or consistency of the oxygen isotope composition of the ocean through time is a crucial parameter in all of these models. Mass balance models have been used to investigate the oxygen isotope composition of the oceans through time, the steady-state condition of the oceans, and the marine chemical sediment problem (Muehlenbachs and Clayton, 1976; Muehlenbachs, 1998; Wallmann, 2001; Jaffres et al., 2007; Sengupta and Pack, 2018). These models consider the processes of high temperature ocean crust alteration, low temperature ocean crust alteration, continental weathering, continental growth, and mantle recycling which result in a net transfer of oxygen between the lithosphere and hydrosphere and collectively buffer the isotopic composition of the oceans. In the present study, we develop a triple oxygen isotope mass balance model for the oceans after the $\delta^{18}O$ model developed in Muehlenbachs (1998) using new $\delta^{18}O$ and $\Delta'^{17}O$ measurements from high and low temperature altered oceanic crust and from basalt-water hydrothermal experiments (Cole et al., 1987).

2. RESULTS AND DISCUSSION

2.1 Altered oceanic crust

Triple oxygen isotope measurements were made for bulk-rock high temperature altered IODP Hess Deep plutonic samples, experimental hydrothermally altered basalts from the run products of Cole et al. (1987), high temperature mineral separates, and low temperature altered DSDP Hole 504B and Hole 417A basalts (**Table 1**, see **Appendix II** for methods). High temperature altered IODP Hess Deep samples show a trend of decreasing $\delta^{18}O$ and increasing $\Delta'^{17}O$ from the pristine mid-ocean ridge value (MORB) (**Fig. 1**). This relationship reflects progressive increases in F/R ratio as sample $\delta^{18}O$ values decrease and $\Delta'^{17}O$ values increase for a given alteration temperature. As F/R ratios increase, the altered rocks approach equilibrium with seawater with an assumed initial $\delta^{18}O = \Delta'^{17}O = 0‰$. Assuming a rock-water isotope fractionation of close to 0‰ for $\delta^{18}O$ and $\delta^{17}O$ values at ~300-400°C, there should be a near linear trend with increasing fluid-rock ratio from unaltered MORB towards pristine ocean water (Schauble and Young, 2021). Our analyses generally fall on this trend. Analysis of chlorite and prehnite high temperature alteration phases also show a similar trend of decreasing $\delta^{18}O$ and increasing $\Delta'^{17}O$ toward seawater and away from primary olivine and plagioclase mineral separate compositions (**Fig. 2**). These results indicate that the $\delta^{18}O$ and $\Delta'^{17}O$ composition of high temperature altered crust can be understood in terms of increases in modal abundance of alteration phases over primary assemblages as whole-rock values approach equilibrium with seawater. Experimentally altered

basalts exchanged with a seawater (initial $\delta^{18}O$ = 1.2‰) show a similar trend to altered Hess Deep samples. If the experimental basalts exchanged with an initial seawater $\delta^{18}O$ = 0‰ this would lower the results by a little less than 0.5‰, bringing the experimental and natural data into excellent agreement and indicating approximate alteration temperatures for Hess Deep samples of ~ 400°C. Low temperature altered basalts exhibit a trend of increasing $\delta^{18}O$ with decreasing $\Delta'^{17}O$ and are indicative of a progressive increases in F/R ratio and low temperature alteration assemblages as sample values diverge from seawater. This process lowers the $\delta^{18}O$ and raises the $\Delta'^{17}O$ of the low temperature phase-producing water altering the rock.

2.2 Ocean buffering mass balance calculations

The oxygen isotope composition of the ocean is presumed to be buffered by F/R interactions during hydrothermal and weathering processes (Muehlenbachs, 1998; Sengupta and Pack, 2018). The ocean buffering mass balance model considers the flux (*F*) of each rock-seawater interaction process, and the corresponding $\delta^{18}O$ and $\delta^{17}O$ fractionations between unaltered and altered lithospheric reservoirs and how they control the $\delta^{18}O$ (and $\Delta'^{17}O$) value of the ocean through time. Fluxes, as well as $\Delta\delta^{18}O$ and $\Delta\delta^{17}O$ equations as a function of seawater $\delta^{17}O$ and $\delta^{18}O$ used in the mass balance model can be found in **Table 2**. Triple oxygen isotope results of high temperature altered plutonic rocks indicate a $\Delta'^{17}O \approx -0.050$‰ for the high temperature altered reservoir corresponding to $\delta^{18}O$ = 4.4‰ and low temperature altered basalt results indicate a $\Delta'^{17}O \approx -0.082$‰ for the corresponding $\delta^{18}O$ = 9.6‰ of the low temperature altered reservoir ($\delta^{18}O$ values from (Muehlenbachs, 1998)).

The modeled ice-free seawater conditions along with Monte Carlo simulated uncertainties for seawater $\delta^{18}O$ and $\Delta'^{17}O$ can be found in **Table 3**. High temperature alteration (*HT*) and continental weathering (*CW*) dominate the $\delta^{18}O$ and $\Delta'^{17}O$ budget of the model where *HT* is responsible for ~ 38% and *CW* is responsible for ~ 36% of all O isotopes transferred. Sensitivity tests examining the effects of varying the $\Delta'^{17}O$ value for the *CW* shale endmember on how seawater compositions evolve from variations in F_{HT} and F_{CW} can be found in **Appendix V**.

Model results shows that the steady state condition of the oceans can be understood in context of lithosphere-hydrosphere interactions that collectively buffer the O isotope composition of the oceans to modern ice-free $\delta^{18}O$ and $\Delta'^{17}O$ estimates. The model predicts a seawater $\delta^{18}O$ = -0.29‰ and $\Delta'^{17}O$ = -0.002‰ that would balance the net $\delta^{18}O$ and $\Delta'^{17}O$ contributions from each geological process with steady state reached at ~ (0.5 to 1)$\times 10^9$ years. The mean model predicted ice-free seawater $\delta^{18}O$ = -0.29‰ is heavier, but close to the expected ice-free $\delta^{18}O$ = -1‰ (e.g., Shackleton and Kennett; 1975). Monte Carlo simulations demonstrate that seawater compositions as low as $\delta^{18}O$ = -0.53‰ within the estimated values for flux uncertainties can be generated by the model. The predicted seawater $\Delta'^{17}O$ = -0.002‰ is an entirely balanced value for an estimated ice-free modern seawater $\Delta'^{17}O \approx 0.004$‰ and demonstrates the efficacy in the model $\delta^{17}O$ and $\delta^{18}O$ inputs to approximate modern ocean conditions. The model can better approximate ice-free ocean conditions if the fluxes are reduced or increased outside of estimated uncertainty bounds. Reduction of F_{HT} by 50% brings the model seawater $\delta^{18}O$ = -1.1‰ and $\Delta'^{17}O$ = 0.001‰, a value in excellent agreement with ice-free $\delta^{18}O$ = -1‰

and $\Delta'^{17}O \approx 0.004‰$. Increasing F_{CW} by 100% brings the model seawater $\delta^{18}O$ = -0.96‰ and $\Delta'^{17}O$ = -0.002‰, again in excellent agreement with ice-free estimates.

2.3 Model predicted seawater compositions

Ancient seawater compositions can be understood through large modifications to F_{HT} to represent geological times with lower sea levels or greater rates of seafloor spreading, and large modifications to F_{CW} to simulate conditions with more or less continents or weathering (Walker and Lohmann, 1989; Wallmann, 2001; Kasting et al., 2006; Jaffres et al., 2007). The effects of modifying F_{HT} and F_{CW} well outside uncertainty bounds on seawater $\delta^{18}O$ and $\Delta'^{17}O$ can be seen in **Fig. 3**. Under conditions with no F_{CW}, the heaviest seawater $\delta^{18}O$ possible is ~ 0.5‰ with a corresponding unchanged $\Delta'^{17}O$ = -0.002‰ and a seawater evolution trend with a slope in $\delta^{17}O$ - $\delta^{18}O$ space λ = 0.528. Decreasing F_{HT} results in the seawater evolution trend with λ = 0.524. Decreasing and shutting off F_{HT} can produce seawater $\delta^{18}O$ values significantly lighter than modern with a minimum $\delta^{18}O$ = -4.1‰ and a corresponding $\Delta'^{17}O$ = 0.014‰. Increasing F_{CW} results in lower seawater $\delta^{18}O$ values that evolve with λ = 0.529 and can reach a minimum seawater $\delta^{18}O$ = -7‰ with corresponding $\Delta'^{17}O$ = 0.005‰. Seawater $\delta^{18}O$ = -7‰ is the lightest the model can generate by modifying a single process and is significantly heavier than the Archean seawater $\delta^{18}O$ = -13.3‰ suggested by Jaffres et al. (2007) by ~ 6‰. Increasing F_{HT} seawater evolves with a λ = 0.524 and can reach a maximum $\delta^{18}O$ = 1.1‰ with a corresponding $\Delta'^{17}O$ = -0.006‰ when F_{HT} is drastically increased. Based on our model, the heaviest seawater $\delta^{18}O$ value that can be obtained is ~

1.1‰ and indicates that heavy Archean seawater $\delta^{18}O$ values suggested by Johnson and Wing (2020) are unattainable.

2.4 Examination of Archean marine chemical sediment data using the model

Model predicted seawater compositions can be used to examine Archean chemical marine sediment equilibration with low seawater $\delta^{18}O$ values. Low Archean seawater $\delta^{18}O$ values such as $\delta^{18}O$ = -13.3‰ suggested by Jaffres et al. (2007) are unobtainable using the model with the lowest $\delta^{18}O$ values from F_{HT} × 0 and F_{CW} × 100 which = -4.1‰ and -7‰, respectively. An Archean Earth environment where F_{CW} is larger than modern estimates due to increased pCO_2 and easily weathered greenstones has been proposed by Jaffres et al. (2007). Shallower Archean oceans and a resulting lower F_{HT} from less seawater percolation through the oceanic crust has been proposed by Walker and Lohmann (1989). To test if ancient marine sediments could have equilibrated with a lighter seawater, the SiO_2 – H_2O equilibrium fractionation curve (Sharp et al., 2016) has been transposed to match our modeled F_{HT} × 0 and F_{CW} × 100 seawater compositions to examine if Archean cherts from Liljestrand et al. (2020), Sengupta et al. (2020), and Lowe et al. (2020) could have equilibrated with our modeled seawaters (**Fig. 4**). All samples from Sengupta et al. (2020) and Liljestrand et al. (2020) plot significantly below our F_{HT} × 0 and F_{CW} × 100 transposed curves, while most chert data from Lowe et al. (2020) plot on or slightly below our F_{HT} × 0 transposed curve and on or above our F_{CW} × 100 transposed curve. Lowe et al. (2020) suggests that well-preserved open

marine, shallow shelf cherts from the Barberton Greenstone Belt (BGB) with no evident metamorphism can potentially indicate Archean ocean surface temperatures. They suggest that these samples are slightly altered from initial $\delta^{18}O$ values ranging from 24 - 26‰ based on their 2σ spread for heavy samples and previous $\delta^{18}O$ work on BGB cherts (Knauth and Lowe, 2003). Sengupta et al. (2020) analyzed BGB cherts (**Fig. 4**) and found samples with a similar range in $\delta^{18}O$ but significantly lighter in $\Delta'^{17}O$ than Lowe et al. (2020), which Lowe et al. (2020) suggests likely indicate metamorphism or diagenesis. Liljestrand et al. (2020) measured nodular and iron formation cherts which have significantly lighter $\Delta'^{17}O$ values and likely reflect diagenesis (Lowe et al., 2020). Cherts precipitating in equilibrium with our modeled F_{HT} × 0 seawater at $\delta^{18}O$ = 26‰ yield a corresponding $\Delta'^{17}O$ = -0.090‰ and a formation temperature of 50°C. Almost all sample data can be explained by chert precipitating in equilibrium with our modeled ocean composition at temperatures of 50 - 60°C and subsequently undergoing some degree of alteration by a meteoric fluid with $\delta^{18}O$ from -7.0 to -20‰ and $\Delta'^{17}O$ from 0.030 to 0.040‰. This precipitation range is 16°C cooler than the estimated range of 66 - 76°C from Lowe et al. (2020). Our F_{CW} × 100 transposed curve fails to account for pristine Lowe et al. (2020) samples since they plot mostly above the curve and cannot be explained by precipitation at higher ocean temperatures or generated through diagenetic mixing models, indicating that lower seawater $\delta^{18}O$ values could not have resulted from an increase in F_{CW}. With the model F_{HT} × 0 generated seawater composition, the Archean chert data can be explained by hotter ocean temperatures (50-60°C), lighter seawater $\delta^{18}O$ than modern, and alteration by a low

$\delta^{18}O$ meteoric water. If Lowe et al. (2020) pristine chert estimates most closely represent the primary Archean cherts compositions in general, then the secular marine chemical sediment trend would reflect varying degrees of sample diagenesis, likely with precipitation in higher ocean temperatures, and lower seawater $\delta^{18}O$ achieved through less hydrothermal seafloor alteration.

Table 1. Triple oxygen isotope analyses of altered oceanic crust and mineral separates.

Sample	$\delta^{17}O$	$\delta^{18}O$	1σ	$\delta'^{17}O$	$\delta'^{18}O$	$\Delta'^{17}O$	1σ	n
504B 70 37-1, 36-38	4.820	9.278	0.08	4.809	9.235	-0.067	0.003	3
504B 70 40-3, 133-135	4.014	7.705	0.40	4.006	7.676	-0.046	0.009	4
504B 70 48-3, 21-23	4.121	7.934	0.28	4.112	7.903	-0.061	0.010	4
51A/417A 32-4, 20-29	7.445	14.359	0.37	7.427	14.257	-0.100	0.008	3
345-U1415J-9R-1, 46-50	2.784	5.396	0.52	2.780	5.381	-0.061	0.009	11
345-U1415J-13R-1, 29-31	1.833	3.575	0.58	1.832	3.568	-0.052	0.009	9
345-U1415J-13R-1, 53-57 (1)	2.384	4.620	0.29	2.381	4.609	-0.052	0.007	4
345-U1415J-13R-1, 53-57 (2)	1.395	2.736	0.14	1.394	2.733	-0.049	0.008	8
345-U1415J-14G-1, 0-6	0.983	1.944	0.29	0.983	1.942	-0.043	0.009	6
345-U1415J-22G-1, 4-8	2.518	4.886	0.25	2.515	4.874	-0.049	0.005	6
1A(300°C)	2.261	4.378	0.23	2.259	4.368	-0.048	0.010	6
2A(400°C)	1.631	3.171	0.12	1.629	3.166	-0.042	0.011	6
2C(400°C)	1.584	3.066	0.12	1.582	3.061	-0.034	0.012	6
2F(400°C)	1.832	3.560	0.15	1.831	3.554	-0.046	0.013	6
6A(500°C)	1.013	1.987	0.23	1.012	1.985	-0.036	0.013	6
3D(500°C)	0.611	1.210	0.23	0.610	1.209	-0.028	0.013	6
345-U1415J-13R-1, 53-57 (Olivine)	2.292	4.450	0.23	2.289	4.440	-0.056	0.016	4
345-U1415J-13R-1, 53-57 (Plagioclase)	2.901	5.596	0.53	2.897	5.580	-0.049	0.010	5
345-U1415J-13R-1, 53-57 (Prehnite)	0.869	1.73	0.18	0.869	1.723	-0.044	0.006	4
HU-120-3 (Chlorite)	0.508	1.002	0.08	0.508	1.002	-0.021	0.009	3

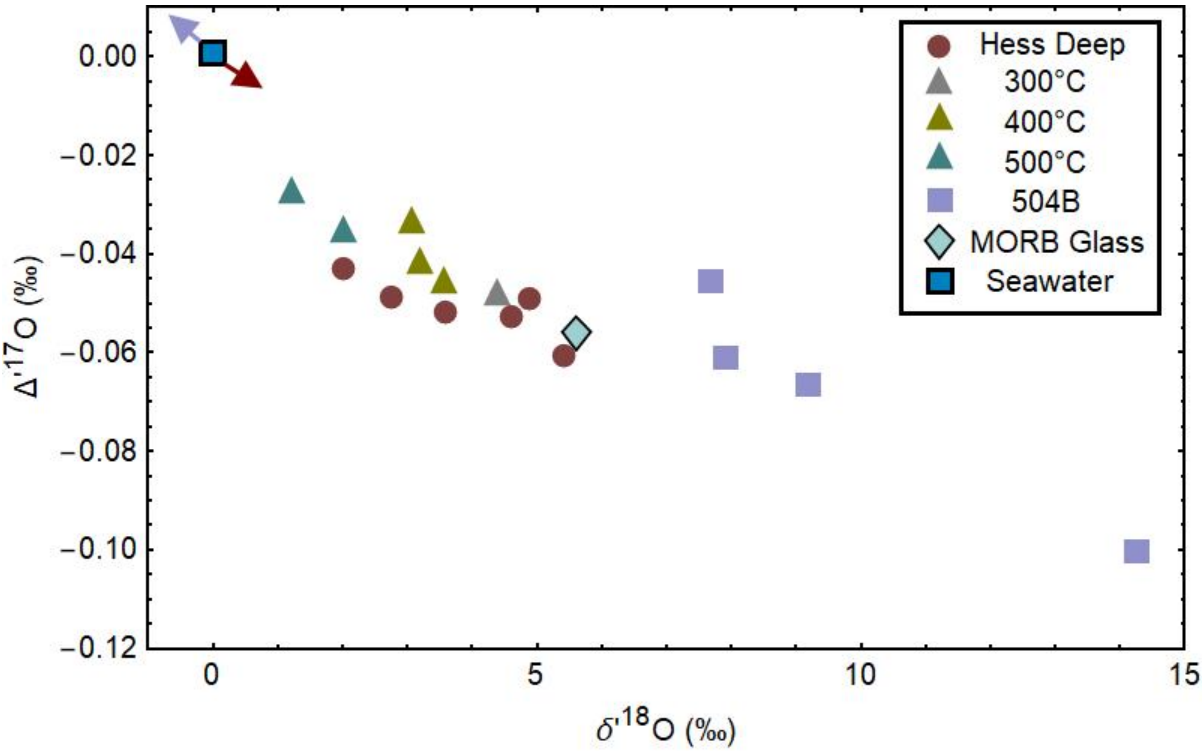

Fig. 1. Plot of Δ'^{17}O vs. δ^{18}O for altered oceanic crust samples. High temperature altered IDOP 345-U1415J samples are represented by brown circles, low temperature altered DSDP Hole 504B and 417A samples are represented by purple squares, and experimental hydrothermally altered basalts are represented by triangles of different colors representing the experimental temperature of alteration. Pristine MORB glass from Cano et al. (2020) is plotted as a diamond as a reference and divider between the low and high temperature alteration paths of altered crust. The modern, steady-state average estimate for seawater is plotted as a square with two protruding arrows representing the effects high and low temperature alteration have on the oxygen isotope composition of seawater. The trend of high temperature alteration of oceanic crust shows a decrease in δ^{18}O and increase in Δ'^{17}O away from MORB and toward seawater. The trend of low temperature alteration of ocean crust shows an increase in δ^{18}O and decrease in Δ'^{17}O away from MORB and seawater. Experimentally altered basalts were altered with seawater of δ^{18}O = 1.2‰ and closely follow the alteration path of IODP 345-U1415J samples. If altered with a seawater of δ^{18}O ≈ Δ'^{17}O ≈ 0‰, samples would shift ~ 0.5‰ to the left and come into excellent agreement with natural data.

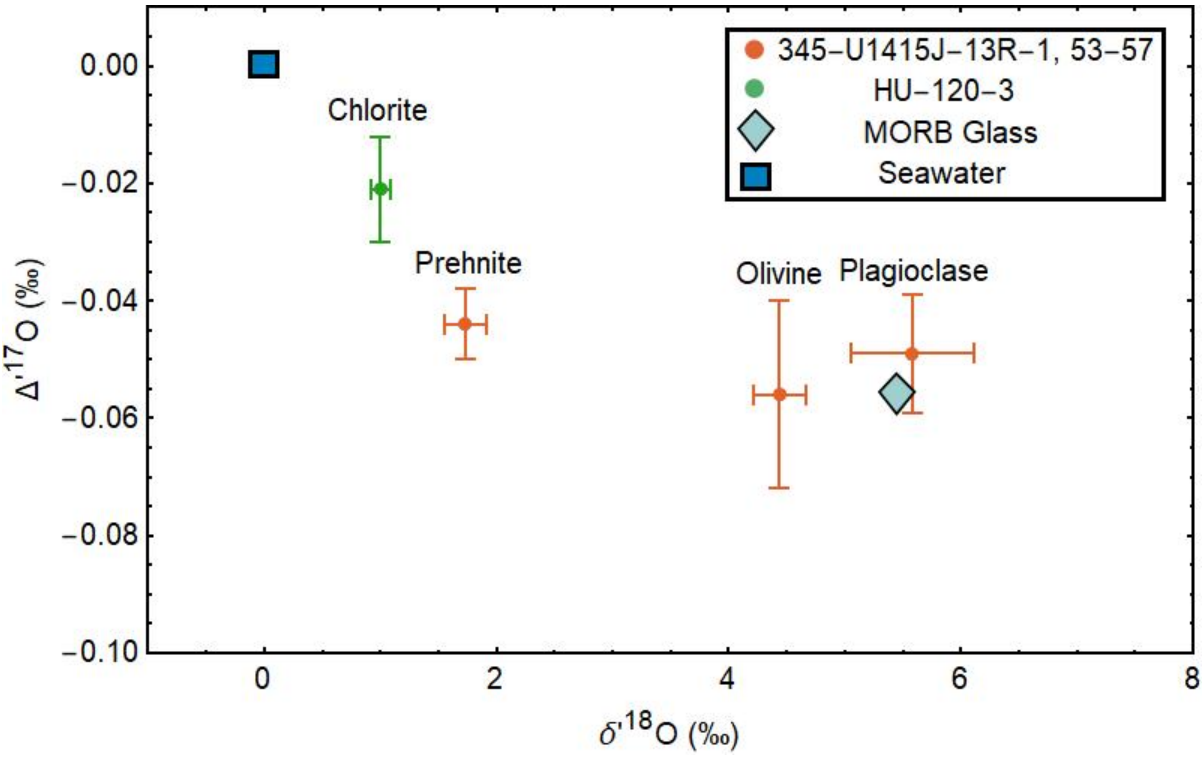

Fig. 2. Plot of Δ'^{17}O vs. δ^{18}O for altered oceanic crust mineral separates. All mineral separate data are represented by circles with horizontal δ^{18}O and vertical Δ'^{17}O error bars. 1σ variation for δ^{18}O ranges from 0.1 to 0.5‰ and 1σ variation for Δ'^{17}O varies from 0.006 to 0.016‰ with n ≥ 3. Primary olivine and plagioclase assemblages were extracted from an olivine-bearing gabbro and show evidence for intense alteration (see **Appendix I**). Alteration assemblages prehnite and chlorite have δ^{18}O and Δ'^{17}O values that approach seawater and show that high temperature altered whole rock sample values can be understood in terms of increases in modal abundance of high temperature alteration phases and F/R ratios.

Table 2. Mass balance model fluxes and Δ equations for each seawater buffering process.

Process	Flux (g/yr)	$\Delta\delta^{17}O$(‰)	$\Delta\delta^{18}O$(‰)
High Temperature Alteration (F_{HT})	1.87×10^{16}	$(2.8 - (\delta^{18}O_{SW} + 2.3))$	$(5.5 - (\delta^{18}O_{SW} + 4.4))$
Low Temperature Alteration (F_{HT})	2.2×10^{15}	$(2.8 - (\delta^{18}O_{SW} + 5.0))$	$(5.5 - (\delta^{18}O_{SW} + 9.6))$
Continental Weathering (F_{CW})	1.02×10^{16}	$-(0.125 \times (5.4 + \delta^{18}O_{SW}) + 0.125 \times (2.8 + \delta^{18}O_{SW}))$	$-(0.125 \times (10.2 + \delta^{18}O_{SW}) + 0.125 \times (5.2 + \delta^{18}O_{SW}))$
Continental Growth (F_{CG})	1.50×10^{15}	$2.9 - ((0.9 \times 2.6) + 0.1 \times (13.5 + \delta^{18}O_{SW}))$	$5.6 - ((0.9 \times 5.1) + 0.1 \times (26.0 + \delta^{18}O_{SW}))$
Mantle Recycling (F_{MR})	0.80×10^{15}	$2.9 - (\delta^{18}O_{SW} + 1.1)$	$5.6 - (\delta^{18}O_{SW} + 2.1)$

Table 3. Monte Carlo simulation result for model predicted seawaters.

Parameters	$\delta^{18}O$	1σ	$\Delta'^{17}O$	1σ	Min $\delta^{18}O$	Max $\delta^{18}O$	Min $\Delta'^{17}O$	Max $\Delta'^{17}O$
Model Seawater	-0.29	0.08	-0.002	0.0003	-0.54	-0.06	-0.002	0.000
50% F_{HT}	-1.10	0.11	0.001	0.0004	-1.41	-0.78	0.000	0.002
150% F_{CW}	-0.96	0.12	-0.001	0.0003	-1.30	-0.65	-0.002	0.000

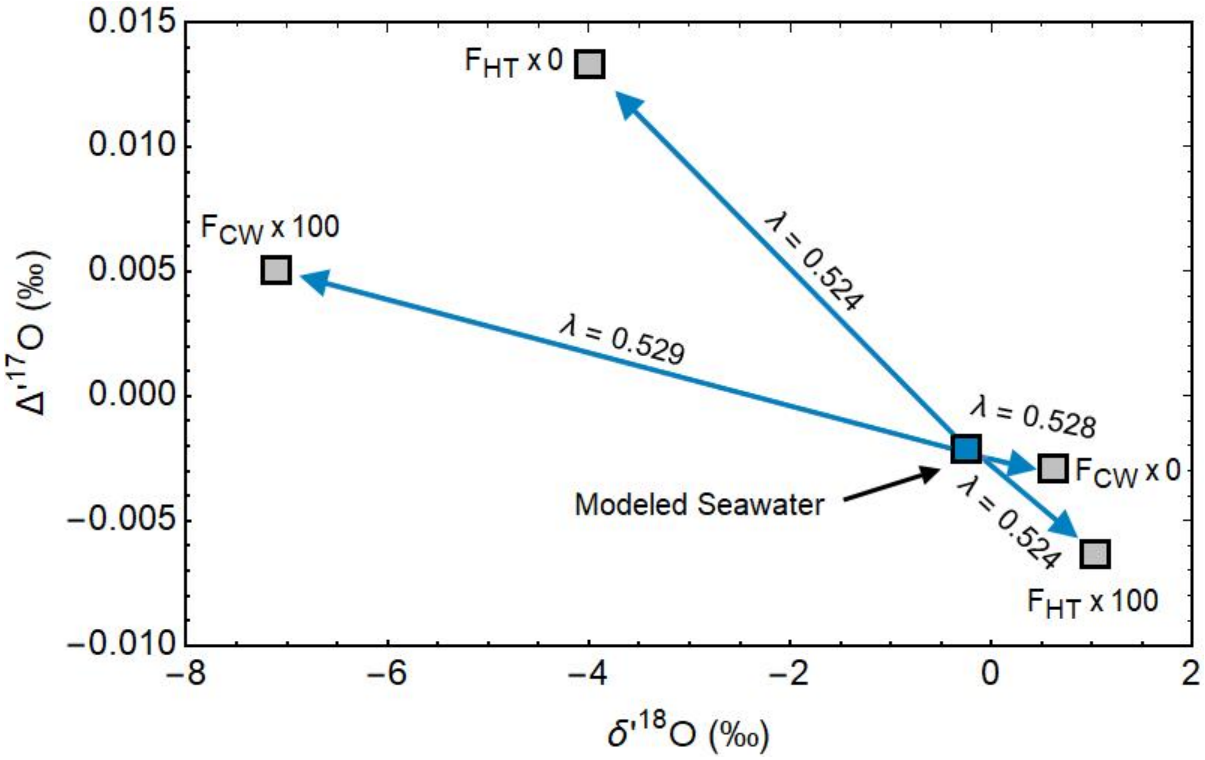

Fig. 3. Plot of evolving seawater compositions as *F_{HT} and F_{CW}* are modified. Blue square represents modeled ice-free seawater (modern conditions), gray squares represent model predicted seawater compositions with different *F_{HT} and F_{CW}* rates. The different rates are signified by $F_i \times x$ where *i* is either the *HT* or *CW* process and *x* is the fractional increase or decrease in the flux. Lighter seawater $\delta^{18}O$ compositions can be achieved by reducing the high-temperature alteration flux (*F_{HT}*) and maximally increasing *F_{CW}* to yield seawater compositions of $\delta^{18}O$ = -4.1‰ and $\Delta'^{17}O$ = 0.014‰, and -7.0‰ and $\Delta'^{17}O$ = 0.005‰, respectively. Heavier seawater $\delta^{18}O$ compositions can be achieved by maximally increasing *F_{HT}* and reducing *F_{CW}* to yield seawater compositions of $\delta^{18}O$ = 1.1‰ and $\Delta'^{17}O$ = -0.006‰, and $\delta^{18}O$ = 0.5‰ and $\Delta'^{17}O$ = -0.002‰, respectively.

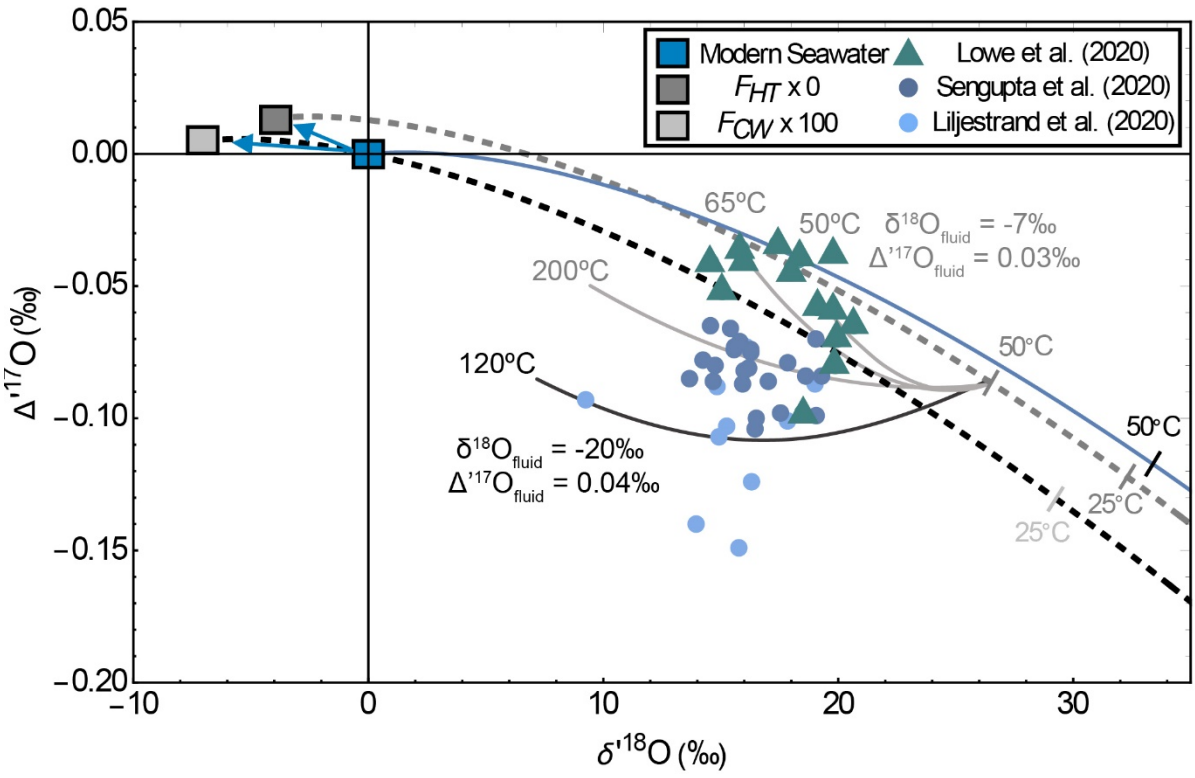

Fig. 4. Plot of modern and model generated seawater compositions with transposed SiO_2–H_2O equilibrium fractionation curves to test Archean chert equilibration with lighter $\delta^{18}O$ seawaters. Blue square represents modern seawater with $\delta^{18}O = \Delta'^{17}O = 0$‰, gray and silver squares represent model generated seawater compositions with $F_{HT} \times 0$ and $F_{CW} \times 100$, respectively, green triangles are Archean chert data from Lowe et al. (2020), while dark and light blue circles are Archean chert data from Sengupta et al. (2020) and Liljestrand et al. (2020), respectively. Lowe et al. (2020) suggest samples have been mildly altered and precipitated in equilibrium with seawater with an initial rock $\delta^{18}O$ between 24 – 26‰. A rock with $\delta^{18}O$ = 26‰ plots with $\Delta'^{17}O$ = -0.084‰ on our transposed $F_{HT} \times 0$ equilibrium curve and has a corresponding formation temperature of 50°C. Diagenetic mixing curves with fluid composition of $\delta^{18}O$ = -7.0‰ and $\Delta'^{17}O$ = 0.03‰, alteration temperatures of 50, 65, and 200°C, and an initial rock composition of $\delta^{18}O$ = 26‰ and $\Delta'^{17}O$ = -0.084‰ (from $F_{HT} \times 0$) are shown in gray. A single mixing curve with a fluid composition of $\delta^{18}O$ = -20.0‰ and $\Delta'^{17}O$ = 0.04‰ and alteration temperature of 120°C is shown in black to account for lighter $\Delta'^{17}O$ samples from Liljestrand et al. (2020). Most chert samples from Lowe et al. (2020) plot above the transposed curve for $F_{CW} \times 100$ and cannot be explained by diagenetic alteration if precipitated in equilibrium with a $F_{CW} \times 100$ seawater composition.

3. CONCLUSIONS

High temperature altered oceanic crust samples show a trend of decreasing $\delta^{18}O$ and increasing $\Delta'^{17}O$ values from pristine MORB glass which can be understood as increases in fluid-rock ratios and hydrous alteration phases as samples approach equilibrium with seawater. This process buffers seawater by increasing the $\delta^{18}O$ and decreasing $\Delta'^{17}O$ during mineral formation. Crustal alteration at low temperatures show a trend of increasing $\delta^{18}O$ and decreasing $\Delta'^{17}O$ from MORB and reflect higher fluid-rock ratios and greater abundances of hydrous alteration phases as sample values diverge from seawater. This processes results in the buffering of seawater to lower $\delta^{18}O$ and $\Delta'^{17}O$ values. The mass balance model after Muehlenbachs (1998) of all seawater buffering processes predicts a seawater composition in excellent agreement with ice-free estimates for the modern ocean, reaching steady state after ~ (0.5 to 1)$\times 10^9$ years, with *HT* and *CW* dominating the exchange budget. Modifications to F_{HT} and F_{CW} produce $\delta^{18}O$ seawater compositions with only minor changes in $\Delta'^{17}O$ (λ_{HT} = 0.524, λ_{CW} = 0.528 - 0.529), with the lowest Archean ocean composition approaching $\delta^{18}O$ values of -7.0‰ and the heaviest approaching 1.1‰. Our λ value for high temperature alteration is significantly higher than that of an earlier model by Sengupta and Pack (2018) and the result is a better fit to the buffering model for a modern ice-free ocean composition. Our altered rock $\delta^{18}O$-$\Delta'^{17}O$ trend also matches data from previous basalt-water exchange experiments (Cole et al., 1987) and fits with published mineral-water (e.g., amphibole and serpentinite) fractionation factors (Schauble and Young, 2021).The triple oxygen isotope data for Archean cherts can be explained as having precipitated in

equilibrium with a seawater $\delta^{18}O$ = -4.1‰ and $\Delta'^{17}O$ = 0.014‰ at temperatures between 50 - 60°C. The low $\delta^{18}O$ and higher $\Delta'^{17}O$ value of the ancient ocean is explained by reducing the amount (flux) of high temperature oceanic crust alteration. An Archean environment with a significantly greater-than-modern F_{CW} does not fit with the least altered Archean samples from Lowe et al. (2020). Almost all Archean chert samples show some evidence of diagenesis, which when corrected for, gives primary equilibration temperatures in the range of 50-60°C.

APPENDICES

Appendix I: Sample Descriptions

Introduction

Hole 504B was drilled into 5.9 Myr old crust approximately 200 km south of the Costa Rica Rift spreading center and is the deepest hole in the oceanic crust, penetrating a depth of 2,111 meters below seafloor (mbsf). The hole is drilled through 274.5 m of sediment, 571.5 m of volcanic rocks, a 209 m volcanic-dike transition zone, and 1056 m of a sheeted dike complex (Alt et al., 1996). Low temperature altered 504B samples analyzed in this study were recovered from the volcanic section of the crust. 504B is the most widely studied oceanic basement core because of the site's unique preservation of alteration phases that record the evolution of hydrothermal alteration systems. Previous oxygen isotope work on volcanic section 504B basalts show a range in $\delta^{18}O$ values from 5.8 to 12.0‰, with most samples falling within the range of 6.1 to 8.5‰ (Alt et al., 1986). All basalts recovered from 504B are tholeiitic and the alteration mineralogy of 504B has been well documented in Alt et al. (1985) and Alt et al. (1996). Propagation of the Cocos-Nazca spreading center westward toward the East Pacific Rise has produced the unique Hess Deep rift valley containing exposed lower crustal magmatic rocks and upper mantle peridotites, as well as upper crustal sheeted dikes and basalt flows. Located near the Pacific, Cocos, and Nazca triple junction, the Hess Deep rift valley was first cored during ODP expedition 147, and later during IDOP expedition 345. All Hess Deep samples analyzed from this study are from Expedition 345 Hole J. Drilling into Hole J was shallow and recovered ~ 26 m from Unit I: rubble, 29.8 m

from Unit II: Oikocryst-Bearing Layered Gabbro Series, and 56 m from Unit III: Troctolites for a total drill depth of 1111.8 mbsf. Samples analyzed in this study are from Unit II and Unit III.

The triple oxygen isotope composition of high temperature altered plutonic rocks and mineral separates from IODP Expedition 345 Hess Deep Core Hole J, low temperature altered basalts from DSDP Expedition 70 Hole 504B and DSDP Expedition 51 Hole 417A, a chlorite mineral separate from the Mid-Atlantic Ridge, and experimentally altered basalts from Cole et al. (1987) were measured to examine basalt-water alteration trends and develop a mass balance model for the oceans. All natural oceanic basalt samples analyzed have been provided by the IODP Gulf Coast Repository, except samples 417A 32-4, 20-29, and HU-120-3 which were provided by Dr. Karlis Muehlenbachs (University of Alberta). Experimental hydrothermally altered basalts have been provided by Dr. David Cole (The Ohio State University). The following sample descriptions only include samples from IODP expedition 345 Hess Deep and DSDP expedition 70 504B. The reader is referred to Cole et al. (1987) for experimental basalts, Muehlenbachs (1980) for 51A/417A 32-4, 20-29, and Muehlenbachs (1972) for HU-120-3 sample descriptions and information. 504B low temperature alteration phases have been identified using Alt et al. (1996) and Hess Deep high temperature alteration phases have been identified using Gillis et al. (2014) as references.

504B sample descriptions

504B 70 37-1 36-38

Sample 504B 70 37-1, 36-38 is an altered basalt comprised of ~ 30% Ca-rich plagioclase, 5% clinopyroxene, 5% orthopyroxene, and 60% alteration assemblages consisting mainly of saponite. Plagioclase occurs as tabular subhedral to euhedral grains, and clinopyroxene and orthopyroxene are anhedral to subhedral. Grain sizes range from fine to medium for plagioclase, and very fine to fine for clinopyroxene, orthopyroxene, and alteration assemblages. Saponite fully replaces clinopyroxene and orthopyroxene and partially replaces plagioclase ubiquitously throughout the sample. Partial replacement of plagioclase, clinopyroxene, and orthopyroxene by minor chlorite is common. Individual Fe-oxyhydroxide veins frequently cut orthopyroxene and clinopyroxene grains, and a single Fe-oxyhydroxide vein cuts through the entire sample.

504B 70 40-3 133-135

Sample 504B 70 40-3, 133-135 is an altered basalt comprised of ~ 45% Ca-rich plagioclase, 30% clinopyroxene, 10% orthopyroxene and 15% secondary assemblages consisting mainly of saponite. Plagioclase occurs as tabular anhedral to subhedral grains, and clinopyroxene and orthopyroxene are anhedral. Grain sizes range from fine to medium for plagioclase, and very fine to fine for clinopyroxene, orthopyroxene, and alteration assemblages. Fine Fe-oxyhydroxide rich halos occur sparsely in patches throughout the sample and often enclosing talc and chlorite, possibly indicating full replacement olivine. Replacement of plagioclase, pyroxene, and orthopyroxene by saponite and minor phillipsite and chlorite is ubiquitous and ranges from mild to intense. Saponite and minor celadonite also occurs in veins

cutting through all primary mineral assemblages. Pyrite is present intermittently throughout the sample and occurs as fine subhedral grains.

504B 70 48-3, 21-23

Sample 504B 70 48-3, 21-21 is an altered basalt comprised of ~ 40% Ca-rich plagioclase, 35% clinopyroxene, 10% orthopyroxene, and 15% alteration assemblages consisting mainly of zeolite. Plagioclase occurs as tabular anhedral grains, and clinopyroxene and orthopyroxene range from anhedral to subhedral. Grain sizes range from fine to medium for plagioclase, and very fine to fine for clinopyroxene, orthopyroxene, and alteration assemblages. Fibrous zeolite is ubiquitous throughout the sample and partially replaces all primary minerals. Intense to complete replacement of orthopyroxene and clinopyroxene by saponite, and minor replacement of all primary minerals by chlorite is common with pyroxene commonly exhibiting > 80% alteration. Partial replacement of plagioclase by celadonite is rare and fine, subhedral oxides are prevalent throughout the sample.

Hess Deep sample descriptions

345-U1415J-9R-1, 46-50

Sample 345-U1415J-9R-1, 46-50 is an altered olivine-bearing gabbro comprised of ~ 35% orthopyroxene, 25% clinopyroxene, 25% plagioclase, 10% olivine, and 5% alteration assemblages consisting mainly of serpentine, chlorite, prehnite, and amphibole. Orthopyroxene, clinopyroxene, and plagioclase are anhedral to subhedral and olivine is subhedral to euhedral. Orthopyroxene, clinopyroxene, and plagioclase grains are coarse to very coarse, and olivine grains are medium to

coarse. Orthopyroxene is mild to intensely altered by chlorite and amphibole, with some grains exhibiting near complete replacement by amphibole. Clinopyroxene is mildly replaced by serpentine, and plagioclase is moderately altered by prehnite and serpentine. Olivine alteration is variable, with some grains exhibiting complete replacement by serpentine and chlorite while some grains are mildly altered by serpentine.

345-U1415J-13R-1, 29-31

Sample 345-U1415J-13R-1, 29-31 is an altered troctolite comprised of ~ 50% Ca-rich plagioclase, 15% olivine, and 35% alteration assemblages consisting mainly of serpentine and unidentifiable clays. Plagioclase occurs as tabular anhedral to subhedral grains, and olivine is anhedral with rare skeletal grains. Grain sizes range from coarse to very course for plagioclase and olivine, and alteration assemblages are fine grained. Serpentine and unidentifiable clay minerals intensely to completely alter olivine, with olivine commonly exhibiting > 90% alteration. Plagioclase is significantly less altered than olivine but is commonly replaced by unidentifiable clays. Serpentine and chlorite veins commonly cut all minerals, and range in size from fine to medium and one medium chlorite veins cuts through the whole sample. Undulose extinction and fracturing are pervasive in plagioclase, indicating substantial sample deformation.

345-U1415J-13R-1, 53-57

Sample 345-U1415J-13R-1, 53-57 is an altered olivine-bearing gabbro comprised mainly of intensely altered plagioclase, olivine, clinopyroxene, and orthopyroxene, with alteration assemblages of prehnite, serpentine, and chlorite

constituting > 80% of the sample. Plagioclase and remnant olivine grains are coarse, clinopyroxene and orthopyroxene are medium to course, and alteration assemblages are medium to coarse grained. Plagioclase is intensely to completely altered by prehnite, and olivine is completely replaced by serpentine. Orthopyroxene and clinopyroxene are replaced by minor chlorite, minor amphibole, and unidentifiable clay minerals. Corona textures are prevalent and consist of aggregate, fine-grained tremolite and chlorite enclosing olivine and plagioclase and make up < 5% of the sample. Prehnite and chlorite veins are ubiquitous, with a single very coarse prehnite vein cut by smaller chlorite veins cutting through the whole sample.

345-U1415J-14G-1, 0-6

Sample 345-U1415J-14G-1, 0-6 is an altered troctolite consisting mainly of intensely altered plagioclase and olivine, with alteration assemblages of serpentine, prehnite, clinozoisite, epidote, chlorite, quartz, and unidentifiable clay minerals constituting > 80% of the sample. Plagioclase and remnant olivine are coarse, while alteration assemblages range in size from very fine (clays, clinozoisite) to fine (serpentine, prehnite, epidote). Plagioclase is mildly to moderately altered by prehnite, clinozoisite, epidote, and clays. Clinozoisite and epidote assemblages appear intergrown and to be replacing both plagioclase and prehnite. Olivine is completely replaced by serpentine and minor clay minerals, with chlorite and secondary quartz occurring adjacent with partially replaced olivine. Prehnite and serpentine veins are ubiquitous and cut both primary mineral grains throughout the whole sample.

345-U1415J-22G-1, 4-9

Sample 345 22-1, 4-9 is an altered gabbronorite comprised of ~ 55% orthopyroxene, 30% plagioclase, 5% clinopyroxene, and 10% alteration assemblages consisting mainly of serpentine, prehnite, chlorite, amphibole, and unidentifiable clay minerals. Orthopyroxene and plagioclase are anhedral and range in grain size from coarse to very coarse, and alteration assemblages are fine grained. Orthopyroxene and clinopyroxene are moderately to intensely altered by serpentine, chlorite, and minor amphibole, and plagioclase is mildly to moderately altered by prehnite and clays. Serpentine veins cut throughout the entirety of the sample and are often accompanied by small cross-cutting chlorite veins. Undulose extinction and fracturing are pervasive in orthopyroxene, indicating substantial sample deformation.

Appendix II: Analytical Methods

O_2 was liberated for mass spectrometric analysis at the University of New Mexico's Center for Stable Isotopes (CSI) using the laser fluorination process of Sharp (1990), as well as the Ni "bomb" method similar to Clayton and Mayeda (1963). High temperature altered crust and mineral separate samples were loaded into a Ni sample block with 44 sample holes and sample sizes ranging from 1.5-3 mg. The chamber was kept under vacuum conditions for approximately 24 hours to achieve high vacuum in the chamber and gas line prior to analysis. Different samples were spaced apart by at least one hole on all sides in the block to prevent contamination during the fluorination process and San Carlos Olivine standards were loaded in each sample block for analysis at the start of each day to ensure calibration of sample runs. The Ni sample block was kept in an isolated 304-stainless steel chamber with a barium window for laser admission under high vacuum conditions and heated with an external halogen lamp overnight to remove any bound water vapor from the samples and chamber. The chamber was then pre-fluorinated with 100 torr BrF_5 for 1 hour at room temperatures to react away any remaining water vapor or other contaminants from the samples.

High temperature altered crustal rocks were fluorinated using 100 torr BrF_5 and heated with a 50 W CO_2 laser until complete fluorination had occurred. Initial beam diameter was large, and the initial laser power was weak, with progressive decreasing of the beam diameter and increasing of the laser power as the sample fluorination progressed. In some instances, the sample chamber was kept at 0°C by placing a dewar filled with ice water under the chamber to examine if passive

reaction was occurring when BrF_5 was introduced into the chamber. Based on San Carlos Olivine standardization analyses at room temperature and 0°C, no evidence was found for passive reaction occurring in Hess Deep gabbros and troctolites. After full fluorination of a sample, excess BrF_5 and silicate fluorination byproducts were removed by cooling a trap with liquid nitrogen. To purify the liberated O_2, the gas was transferred through a trap cooled with liquid nitrogen, followed by a NaCl trap heated to approximately 100°C, followed by a final cooled trap to remove any fluorination products. O_2 was subsequently transferred into a 5 Å mol sieve trap filled using zeolites for the adsorption of O_2 under liquid nitrogen conditions. The sieve trap was then heated, and the sample gas was carried through a gas chromatography column (5A mol sieve) carried by a purified He stream at a constant flow rate of 5.0 ml/min to remove any traces of NF_3 that could interfere with the ^{17}O signal in the mass spectrometer. The sample was then collected in a second 5 Å mol sieve filled with zeolites cooled under liquid nitrogen conditions at the inlet of a Thermo-Finnegan MAT 253 dual-inlet isotope ratio mass spectrometer. Transfer of O_2 gas was monitored using a homemade thermal conductivity detector. Prior to analysis, excess He in the trap was pumped away and the O_2 was then transferred into the bellows of the mass spectrometer.

Analysis of reactive low temperature altered basalts instead underwent fluorination using the “Ni bomb” method due to potential passive reaction occurring when BrF_5 was introduced into the sample chamber during the laser fluorination process. For this method, samples were loaded into Ni tubes and heated at 100 °C for 1 hour to remove any water vapor from the samples and the walls of the tubes.

100 torr BrF_5 was then introduced into the tubes which were subsequently heated to 600°C and reacted overnight. After full fluorination has occurred, the tubes were cooled using liquid nitrogen to remove remaining BrF_5 and residual fluorination products. The liberated O_2 was then released into the O_2 gas line and purified using the same procedure described above.

All Thermo-Finnegan MAT 253 mass spectrometer operations, sample and reference bellow calibrations, and recordings of each analysis were conducted in Isodat 3.0 Acquisition. The intensities of both the sample and reference gas were matched with adjustments to bellow compression levels to obtain intensities between 3.0 – 4.0 volts for each sample run. The CSI reference gas used for each analysis is calibrated relative to the VSMOW2-SLAP2 scale as described in Wostbrock et al. (2020). Oxygen isotope ratios were measured on masses 32, 33 and 34 using long collection times of 26 seconds with 30 iterations occurring per analysis against the O_2 reference gas to achieve the desired high precision necessary to measure the triple oxygen isotopes of samples. Reproducibility on the UNM San Carlos olivine standard are 0.16‰ for $\delta^{18}O$ and 0.014‰ for $\Delta'^{17}O$ (Sharp and Wostbrock, 2021).

Prior to analysis, whole-rock samples were powdered in a steel mortar and pestle to ensure homogenization of highly heterogeneous rocks. Precipitate carbonate assemblages were removed from whole-rock samples by hand to eliminate CO_2 liberation during the fluorination process. CO_2 is estimated to only constitute 2.5% of the oceanic crust and is not a significant enough component to consider in the low temperature basalt alteration process within the mass balance model (Coogan and Gillis, 2013; Coogan and Dosso, 2015). Plagioclase and olivine were separated from

sample 345 13-1, 53-57 for analysis using a Frantz Isodynamic Magnetic Separator and hand picking.

Appendix III: Triple Oxygen Isotope Systematics

All triple oxygen isotope results are reported in per mil notation and relative to the VSMOW2 scale where:

$$\delta = \left(\frac{R_x}{R_{std}} - 1\right) \times 1000 \quad (1)$$

and

$$\delta' = 1000 \times \ln\left(\frac{\delta}{1000} + 1\right) \quad (2)$$

and R_x is the ratio of the heavy to light isotope of any sample x and R_{std} is the ratio of the heavy to light isotope of the standard (McKinney et al., 1950). To measure small deviations from a reference line (RL) used to approximate the terrestrial fractionation line (TFL), the $\Delta'^{17}O$ notation has been introduced and is defined as:

$$\Delta'^{17}O = \delta'^{17}O - \lambda_{RL} \times \delta'^{18}O + \gamma_{RL} \quad (3)$$

where λ_{RL} is the slope and γ_{RL} is the y-intercept of the reference fractionation line in $\delta^{17}O$- $\delta^{18}O$ space. This study uses the $\lambda_{RL} = 0.528$ convention and considers $\gamma_{RL} = 0$. For thermodynamic equilibrium fractionation processes between two phases, the slope λ is replaced by θ to signify an equilibrium process in the triple oxygen isotope system where θ is defined by:

$$\theta_{A\text{-}B} = \frac{\delta'^{17}O_A - \delta'^{17}O_B}{\delta'^{18}O_A - \delta'^{18}O_B} \quad (4)$$

and A and B are any two phases in equilibrium.

Although there are three stable isotopes of oxygen, it has traditionally been the convention in stable isotope geochemistry to measure only the $\delta^{18}O$ value of a material since it has long been recognized that the $^{17}O/^{16}O$ ratio is approximately

half the $^{18}O/^{16}O$ ratio (Craig, 1957). The equilibrium fractionation between two substances A and B with respect to ^{17}O and ^{18}O is given by:

$$\alpha^{17}O_{A\text{-}B} = (\alpha^{18}O_{A\text{-}B})^{\theta} \quad (5)$$

where $\alpha_{A\text{-}B} = R_A/R_B$ for any two phases A and B and θ is approximately 0.5. This correlation implies that $\delta^{17}O$ measurements will provide no additional information and are superfluous. Equilibrium fractionation is a temperature dependent process and the fractionation between two phases approaches 0‰ at infinite temperatures. Variations in θ are responsible for the mass dependent fractionation trends observed in triple oxygen isotope measurements. Like the equilibrium fractionation factor α, θ is a temperature dependent variable. That these variations exist in θ despite all Earth materials possibly originating from a single homogenized source reflects the isotopic influence of the different processes through which these materials evolved. It is through calculations of θ at various temperatures that equilibrium fractionation relationships between any two phases are determined.

The relationship between $\delta^{18}O$ and $\delta^{17}O$ can be defined in cartesian space and plotted along a single line known as the terrestrial fractionation line (TFL), defined by the expression:

$$\delta'^{17}O = \lambda_{TFL} \times \delta'^{18}O + \gamma_{TFL} \quad (6)$$

where λ_{TFL} is the slope and γ_{TFL} is the y-intercept of the TFL – a chosen best fit line with a slope approximately equal to 0.5. Examining a sample's deviation from the TFL is common in meteorite studies to characterize and classify relationships between different extraterrestrial bodies and their locations in the solar systems. These deviations are often large and can be recognized through relatively low

precision oxygen isotopic measurements. Recently it has been shown that there exists small deviations from the TFL in terrestrial samples that are the result of mass-dependent fractionation processes (Luz and Barkan, 2010; Pack and Herwartz, 2014). These deviations are often small and require oxygen isotope measurements at high precision that can now be obtained due to recent methodological and technological improvements. Small deviations from the TFL are best visualized through use of $\Delta'^{17}O$ notation, calculated relative to a reference line (see **equation 3**). It is important to recognize that $\Delta^{17}O$ is a calculation based on $\delta^{18}O$ and $\delta^{17}O$ measurements, not itself a measurement, and the λ_{RL} value is not strictly defined and must be chosen. This study uses a $\lambda_{RL} = 0.528$ and $\gamma_{RL} = 0$. A $\lambda_{RL} = 0.528$ is an arbitrary value that has not been used unanimously across the triple oxygen isotope community but is chosen in part to graphically resolve the meteoric water trend in $\delta^{18}O$ - $\Delta^{17}O$ space to a slope of ≈ 0 (see Sharp, (2018) for a detailed explanation on choosing $\lambda_{RL} = 0.528$).

Appendix IV: Data

All analyses made for altered oceanic crustal samples and mineral separates are reported here. If sample run values for $\delta^{18}O$ or $\Delta'^{17}O$ are beyond 3σ, the run was not included in the mean calculation. Sample 345-U1415J-13R-1, 53-57 appeared highly heterogenous with respect to alteration and was run using two different sections of the same sample ((1) and (2)). Sample 345-U1415J-22G-1, 4-8 runs 1 through 3 were corrected by +0.02 for $\Delta'^{17}O$ based on light $\Delta'^{17}O$ SCO standards that day. All data are reported in per mil notation relative to VSMOW with a $\delta^{18}O$ and $\delta^{17}O$ value of 0‰. $\Delta'^{17}O$ values are calculated using a λ value of 0.528.

Table 4. Low temperature altered oceanic crust samples runs.

Sample	$\delta^{17}O$	$\delta^{18}O$	$\delta'^{17}O$	$\delta'^{18}O$	$\Delta'^{17}O$
504B 70 37-1, 36-38	4.809	9.255	4.797	9.213	-0.067
	4.873	9.371	4.861	9.327	-0.064
	4.781	9.208	4.769	9.166	-0.070
Mean	4.821(± 0.04)	9.278(± 0.08)	4.809	9.235	-0.067(± 0.003)
504B 70 40-3, 133-135	4.027	7.713	4.019	7.683	-0.038
	3.853	7.388	3.845	7.361	-0.041
	3.883	7.459	3.875	7.431	-0.048
	4.295	8.261	4.286	8.227	-0.058
Mean	4.014(± 0.17)	7.705(± 0.40)	4.006	7.676	-0.046(± 0.009)
504B 70 48-3, 21-23	4.308	8.309	4.299	8.275	-0.070
	3.980	7.643	3.972	7.614	-0.049
	4.093	7.872	4.084	7.841	-0.056
	4.102	7.912	4.093	7.881	-0.068
Mean	4.121(± 0.11)	7.934(± 0.28)	4.112	7.903	-0.061(± 0.010)
51A/417A 32-4, 20-29	7.626	14.704	7.597	14.596	-0.110
	7.256	13.976	7.230	13.879	-0.098
	7.483	14.398	7.455	14.296	-0.093
Mean	7.455(± 0.15)	14.359(± 0.37)	7.427	14.257	-0.100(± 0.008)

Table 5. High temperature altered oceanic crust sample runs.

Sample	$\delta^{17}O$	$\delta^{18}O$	$\delta'^{17}O$	$\delta'^{18}O$	$\Delta'^{17}O$
345-U1415J-9R-1, 46-50	3.147	6.078	3.142	6.059	-0.057
	3.107	6.009	3.102	5.991	-0.061
	3.081	5.691	3.076	5.675	0.080
	2.863	5.558	2.859	5.543	-0.068
	3.010	5.819	3.005	5.802	-0.058
	2.963	5.774	2.958	5.757	-0.081
	2.442	4.746	2.439	4.735	-0.061
	2.448	4.740	2.445	4.729	-0.052
	2.520	4.878	2.517	4.866	-0.052
	2.563	4.988	2.560	4.976	-0.067
	2.777	5.369	2.773	5.355	-0.054
Mean	2.784(± 0.27)	5.396(± 0.52)	2.780	5.381	-0.061(± 0.009)
345-U1415J-13R-1, 29-31	1.967	3.843	1.965	3.836	-0.060
	1.933	3.737	1.931	3.730	-0.038
	2.061	4.017	2.059	4.009	-0.058
	2.102	4.092	2.100	4.084	-0.056
	2.122	4.126	2.120	4.117	-0.054
	1.294	2.568	1.293	2.565	-0.061
	1.501	2.922	1.500	2.918	-0.041
	1.667	3.187	1.666	3.182	-0.014
	1.690	3.291	1.689	3.286	-0.046
Mean	1.834(± 0.29)	3.575(± 0.58)	1.832	3.568	-0.052(± 0.009)
345-U1415J-13R-1, 53-57 (1)	2.569	4.982	2.566	4.970	-0.058
	2.395	4.651	2.392	4.640	-0.058
	2.204	4.263	2.202	4.254	-0.045
	2.369	4.582	2.366	4.572	-0.048
Mean	2.384(± 0.13)	4.620(± 0.29)	2.381	4.609	-0.052(± 0.007)

Table 5 (cont.).

Sample	$\delta^{17}O$	$\delta^{18}O$	$\delta'^{17}O$	$\delta'^{18}O$	$\Delta'^{17}O$
345-U1415J-13R-1, 53-57 (2)	1.336	2.645	1.336	2.641	-0.059
	1.400	2.743	1.399	2.740	-0.048
	1.366	2.691	1.365	2.687	-0.054
	1.484	2.826	1.483	2.822	-0.007
	1.497	2.928	1.496	2.924	-0.048
	1.494	2.918	1.493	2.914	-0.045
	1.329	2.619	1.328	2.616	-0.053
	1.342	2.610	1.341	2.607	-0.035
Mean	1.395(± 0.07)	2.736(± 0.14)	1.394	2.733	-0.049(± 0.008)
345-U1415J-14G-1, 0-6	1.057	2.062	1.056	2.060	-0.031
	1.222	2.393	1.221	2.390	-0.041
	0.331	0.714	0.331	0.714	-0.046
	0.912	1.825	0.912	1.823	-0.051
	0.827	1.667	0.827	1.666	-0.053
	0.897	1.773	0.897	1.771	-0.039
Mean	0.983(± 0.14)	1.944(± 0.29)	0.983	1.942	-0.043(± 0.009)
345-U1415J-22G-1, 4-8	2.607	5.073	2.603	5.060	-0.048
	2.561	4.998	2.558	4.986	-0.055
	2.481	4.825	2.478	4.814	-0.044
	2.619	5.049	2.616	5.036	-0.043
	2.562	4.957	2.559	4.945	-0.052
	2.278	4.412	2.275	4.402	-0.049
Mean	2.518(± 0.12)	4.886(± 0.25)	2.515	4.874	-0.048(± 0.005)

Table 6. Experimental hydrothermally altered oceanic basalt sample runs.

Sample	$\delta^{17}O$	$\delta^{18}O$	$\delta'^{17}O$	$\delta'^{18}O$	$\Delta'^{17}O$
1A(300°C)	2.336	4.534	2.333	4.524	-0.055
	2.447	4.744	2.444	4.733	-0.055
	2.239	4.320	2.236	4.311	-0.040
	2.305	4.427	2.302	4.417	-0.030
	2.079	4.039	2.077	4.031	-0.051
	2.162	4.204	2.160	4.195	-0.055
Mean	2.261(± 0.12)	4.378(± 0.23)	2.259	4.368	-0.048(± 0.010)
2A(400°C)	1.624	3.180	1.623	3.175	-0.054
	1.638	3.170	1.637	3.165	-0.034
	1.674	3.225	1.673	3.220	-0.027
	1.498	2.984	1.497	2.980	-0.076
	1.716	3.324	1.715	3.318	-0.038
	1.502	2.955	1.501	2.951	-0.057
Mean	1.631(± 0.07)	3.171(± 0.12)	1.629	3.166	-0.042(± 0.011)
2C(400°C)	1.537	2.975	1.536	2.971	-0.033
	1.552	2.985	1.551	2.981	-0.023
	1.634	3.120	1.633	3.115	-0.012
	1.719	3.295	1.718	3.290	-0.019
	1.550	3.035	1.549	3.030	-0.051
	1.560	3.039	1.559	3.034	-0.043
Mean	1.584(± 0.07)	3.066(± 0.12)	1.582	3.061	-0.034(± 0.012)

Table 6 (cont.).

Sample	$\delta^{17}O$	$\delta^{18}O$	$\delta'^{17}O$	$\delta'^{18}O$	$\Delta'^{17}O$
2F(400°C)	1.808	3.492	1.806	3.486	-0.034
	1.917	3.720	1.915	3.713	-0.045
	1.881	3.648	1.879	3.641	-0.043
	1.830	3.525	1.828	3.519	-0.030
	1.682	3.290	1.681	3.285	-0.054
	1.876	3.685	1.874	3.678	-0.068
Mean	1.832(± 0.08)	3.560(± 0.15)	1.831	3.554	-0.046(± 0.013)
6A(500°C)	1.043	2.069	1.042	2.067	-0.049
	1.106	2.144	1.105	2.142	-0.025
	1.186	2.293	1.185	2.290	-0.024
	1.068	2.050	1.067	2.048	-0.014
	0.872	1.705	0.872	1.704	-0.028
	0.856	1.724	0.856	1.723	-0.054
Mean	1.013(± 0.13)	1.987(± 0.23)	1.012	1.985	-0.036(± 0.013)
3D(500°C)	0.453	0.924	0.453	0.924	-0.035
	0.733	1.425	0.733	1.424	-0.019
	0.596	1.181	0.596	1.180	-0.027
	0.468	0.899	0.468	0.899	-0.007
	0.710	1.400	0.710	1.399	-0.029
	0.704	1.428	0.704	1.427	-0.050
Mean	0.611(± 0.11)	1.210(± 0.23)	0.610	1.209	-0.028(± 0.013)

Table 7. High temperature alteration phase mineral separate runs.

Sample	$\delta^{17}O$	$\delta^{18}O$	$\delta'^{17}O$	$\delta'^{18}O$	$\Delta'^{17}O$
345-U1415J-13R-1, 53-57 (Olivine)	2.295	4.463	2.292	4.453	-0.059
	2.411	4.668	2.408	4.657	-0.051
	2.317	4.535	2.314	4.525	-0.075
	2.143	4.134	2.141	4.125	-0.038
Mean	2.292(± 0.10)	4.450(± 0.23)	2.289	4.440	-0.056(± 0.016)
345-U1415J-13R-1, 53-57 (Plagioclase)	2.924	5.652	2.920	5.636	-0.056
	3.192	6.155	3.187	6.136	-0.053
	2.971	5.700	2.967	5.684	-0.034
	2.518	4.875	2.515	4.863	-0.053
	2.446	4.690	2.443	4.679	-0.028
Mean	2.901(± 0.24)	5.596(± 0.53)	2.897	5.580	-0.049(± 0.010)
345-U1415J-13R-1, 53-57 (Prehnite)	0.998	1.988	0.998	1.986	-0.051
	0.825	1.639	0.825	1.638	-0.040
	0.799	1.601	0.799	1.600	-0.046
	0.854	1.692	0.854	1.691	-0.039
Mean	0.869(± 0.08)	1.730(± 0.18)	0.869	1.728	-0.044(± 0.006)
HU-120-3 (Chlorite)	0.530	1.044	0.530	1.043	-0.021
	0.547	1.059	0.547	1.058	-0.012
	0.448	0.905	0.448	0.904	-0.030
Mean	0.508(± 0.04)	1.002(± 0.08)	0.508	1.002	-0.021(± 0.009)

Appendix V: The Mass Balance Model

Lithosphere-hydrosphere interactions that result in the net transfer of oxygen isotopes has been shown to buffer the oxygen isotope composition of the oceans to the modern steady state $\delta^{18}O$ value of 0‰ (Muehlenbachs and Clayton, 1976; Muehlenbachs, 1998). Muehlenbachs and Clayton (1976) developed a mass balance model for the Earth's oceans using the $\delta^{18}O$ values of the analyzed altered basalts. In this model, four geologic processes are hypothesized to actively buffer the oxygen isotope composition of seawater: continental weathering, low temperature alteration of oceanic lithosphere, hydrothermal alteration of oceanic lithosphere, and water recycling – each of which contribute to the $\delta^{18}O$ value of seawater by functioning as a source or sink for the heavy oxygen isotope. Muehlenbachs (1998) later revised this model to incorporate the process of continental growth and adjust the high and low temperature basalt alteration parameters. The mass balance model is used to calculate the total oxygen isotopic exchange resulting from hydrosphere-lithosphere interactions by considering the oxygen flux between reservoir and ocean and the isotopic fractionation between starting and altered reservoir. The result of the model indicate that if the considered processes operated the same way over a billion years, there is only a net contribution of approximately -0.1‰ to the $\delta^{18}O$ value of seawater, a result lighter than the estimated $\delta^{18}O$ = -1‰ value of ice-free conditions (Shackleton and Kennett, 1975). Other box models considering oxygen isotope exchange processes occurring within the geological water cycle have found that early Earth oceans had a low $\delta^{18}O$

value that was progressively raised over time from changes in the ratio of high to low temperature alteration processes (Wallmann, 2001; Jaffres et al., 2007).

Sengupta and Pack (2018) presented a triple oxygen isotope mass balance model for the oceans adopted from the $\delta^{18}O$ model by Muehlenbachs (1998). The study measured the triple oxygen isotope composition of altered oceanic basalts, as well as a marine shale, and developed a model for both $\delta^{18}O$ and $\delta^{17}O$. Their results show a trend of decreasing $\delta^{18}O$ with increasing $\Delta'^{17}O$ for high temperature altered crust ($\theta_{basalt\text{-}water} = 0.5273$) and a trend of increasing $\delta^{18}O$ with decreasing $\Delta'^{17}O$ for low temperature altered crust ($\theta_{basalt\text{-}water} = 0.5247$). The mass balance model shows that ice-free ocean conditions can be achieved with adjustments to the continental weathering and hydrothermal alteration fluxes. A predicted seawater evolution trend in $\delta'^{18}O - \Delta'^{17}O$ space was modeled through high magnitude flux variations to examine if ancient marine chert data could be in equilibrium with a model predicted low $\delta^{18}O$ seawater composition. Translation of the triple oxygen isotope equilibrium fractionation curve for the $SiO_2 - H_2O$ system determined in Sharp et al. (2016) to the model predicted low $\delta^{18}O$ seawater value suggest that Archean chert triple oxygen isotope data from Levin et al. (2014) could not be in equilibrium with a low $\delta^{18}O$ seawater and are best explained by diagenetic alteration.

The $\delta^{18}O$ mass balance model for the oceans originally developed by Muehlenbachs and Clayton (1976) revolutionized the stable isotope geochemistry community's understanding of the oxygen isotope composition of seawater. This was the first model to propose to explain why and how the oxygen isotope composition of seawater is buffered to its modern steady state value of $\delta^{18}O = 0‰$,

and many studies since, including this one, have sought to examine the implications of the original paper using new data and some model modifications. The models with the most substantial modifications come from Wallmann (2001) and Jaffres et al. (2007) which consider H_2O fluxes and ^{18}O transfer between reservoirs and was constructed assuming the ancient marine carbonate trend reflects the evolution of seawater $\delta^{18}O$ to heavier values over time. This study uses a method similar to Muehlenbachs (1998) but examines the solution for seawater $\delta^{18}O$ and $\Delta'^{17}O$ that would balance the contributions of each process (also the approach of Sengupta and Pack (2018)) as opposed to the net contributions each process has on the oxygen isotope composition of seawater. The distinction between the two different approaches is important because the assumptions and net results of running the model are different for both. Muehlenbachs (1998) assumes $\delta^{18}O = 0‰$ and the model can be used to examine the total contribution each process has on seawater $\delta^{18}O$ given this assumption. The approach used by Sengupta and Pack (2018) and this study does not assume seawater $\delta^{18}O = 0‰$ but that the oceans are in steady state and that a solution exists for seawater $\delta^{18}O$ and $\Delta'^{17}O$ that balances the contributions of each process.

The mass balance model used in this study, along with all flux (*F*) estimates and most reservoir $\delta^{18}O$ values, was developed after Muehlenbachs (1998). The model considers five geological processes that buffer the oxygen isotope composition of the oceans through hydrosphere-lithosphere interactions:

1. High temperature alteration of oceanic crust (*HT*)
2. Low temperature alteration of oceanic crust (*LT*)

3. Weathering of continents (*CW*)

4. Continental growth by sediment recycling (*CG*)

5. Mantle recycling of subducted water (*MR*)

The mass balance model calculates a seawater $\delta^{18}O$ and $\Delta'^{17}O$ that can balance the $\delta^{17}O$ and $\delta^{18}O$ contributions to the O isotope composition of seawater from each process and was run according to the following equations:

$$\frac{\partial}{\partial t}\delta^{18}O_{seawater} = 10^9 \text{ (yrs)} \times \sum \frac{F_i}{M_{ocean}} \times \Delta(\delta^{18}O_i) \quad (7)$$

and

$$\frac{\partial}{\partial t}\delta^{17}O_{seawater} = 10^9 \text{ (yrs)} \times \sum \frac{F_i}{M_{ocean}} \times \Delta(\delta^{17}O_i) \quad (8)$$

where F_i = the flux of buffering process *i* (g/yr) and M_{ocean} = the total mass of oxygen in the ocean (g). The model processes buffer the $\delta^{17}O$ and $\delta^{18}O$ values of seawater through seawater-rock interactions that result in a net oxygen isotope exchange and produce an altered lithospheric reservoir. Running the model by 10^9 years is used to approximate the time it takes for the seawater to reach steady state but is an arbitrary constant. Sengupta and Pack (2018) found their model to reach steady state after 2.6×10^8 years, while Muehlenbachs (1998) found the model to reach steady state after 10^9 years. The Δ value quantifies the fractionation between unaltered and altered reservoir for each process where:

$$\Delta(\delta^{18}O_i) = \delta^{18}O_i^{unaltered} - \delta^{18}O_i^{altered} \quad (9)$$

and

$$\Delta(\delta^{17}O_i) = \delta^{17}O_i^{unaltered} - \delta^{17}O_i^{altered} \quad (10)$$

$\delta^{17}O$ and $\delta^{18}O$ values for altered and unaltered reservoirs are determined though measurements and estimations used to approximate the global averages for each

reservoir. $\Delta'^{17}O$ measurements of altered oceanic crust from this study are used to determine $\delta^{17}O_{HT}^{altered}$ and $\delta^{17}O_{LT}^{altered}$, and all other reservoir $\delta^{17}O$ values are taken from Sharp et al. (2016), Bindeman et al. (2018), Sengupta and Pack (2020), and Cano et al. (2020). The five geological processes and triple oxygen isotope compositions of reservoirs in the model are considered as follows:

High temperature alteration of oceanic crust (*HT*) lowers the $\delta^{18}O$ and raises the $\Delta'^{17}O$ value of lithosphere from its unaltered $\delta^{18}O \approx 5.5 - 5.8‰$ and $\Delta'^{17}O \approx -0.057‰$ to an average altered $\delta^{18}O \approx 4.4‰$ from the migration of water through hot (estimated 300–500 °C), newly formed oceanic lithosphere (Muehlenbachs, 1998; Sengupta and Pack, 2018; Cano et al., 2020). A corresponding altered reservoir $\Delta'^{17}O = -0.008‰$ ($\lambda = 0.528$) was determined by Sengupta and Pack (2018) based on high temperature altered DSDP/ODP hole 504B basalts. The triple oxygen isotope results from IODP Hess Deep plutonic samples indicate a corresponding $\Delta'^{17}O = -0.05‰$, significantly different that the findings of Sengupta and Pack (2018). Hot seawater migration through the crust is estimated to affect up to 5 km of the oceanic lithosphere with F_{HT} being the largest in model by approximately a factor of two. Formation of low $\delta^{18}O$ and $\Delta'^{17}O$ greenstone alteration phases from high temperature fluid-rock interaction enriches the oceans in $\delta^{18}O$ and depletes the oceans in $\Delta'^{17}O$. Changing the average *HT* altered reservoir to our *HT* data average of $\delta^{18}O = 3.60‰$ and $\Delta'^{17}O = -0.045‰$ in the model yields a modeled seawater of $\delta^{18}O = 0.30‰$ and $\Delta'^{17}O = -0.007‰$, a value significantly heavier than expected for ice-free conditions..

Low temperature alteration of oceanic crust (*LT*) results from the percolation of cold seawater through cooled, off-axis crust which raises the $\delta^{18}O$ and lowers the $\Delta'^{17}O$ of the unaltered oceanic lithosphere to an average $\delta^{18}O \approx 9.6‰$ (Muehlenbachs, 1998; Sengupta and Pack, 2018). Sengupta and Pack (2018) found the corresponding altered $\Delta'^{17}O = -0.098‰$ ($\lambda = 0.528$) based on low temperature altered IODP hole U1383C basalts. This study found a heavier corresponding *LT* $\Delta'^{17}O = -0.082‰$ based on measurements of DSDP hole 504B and hole 417A basalts. Percolation of cold seawater through the lithosphere is shallow and is estimated to affect only the upper 600 m of the crust and results in a low $F_{LT} \approx 1/9$ F_{HT}. Low temperature alteration of oceanic basalt forms hydrous clay minerals with large $\delta^{18}O$ and low $\Delta'^{17}O$ values and depletes the oceans in $\delta^{18}O$ and enriches the oceans in $\Delta'^{17}O$. Fractionation between seawater and reservoir is a function of the reaction temperature and the oxygen isotope composition of the seawater and reservoir. Keeping the Δ equations as a function of seawater allows for examination of the contributions from each process with different seawater $\delta^{18}O$ and $\Delta'^{17}O$ compositions.

Weathering of continents (*CW*) results from interaction between continental lithosphere and low $\delta^{18}O$ meteoric water, raising the $\delta^{18}O$ and lowering the $\Delta'^{17}O$ of the continents. The flux estimate considers the present-day river sediment load containing 50% recycled sediment (not net $\delta^{18}O$ or $\Delta'^{17}O$ transfer), 25% weathered igneous crust, and 25% weathered metamorphic crust. The modeled process estimates a weathered crustal reservoir to be a shale with $\delta^{18}O = 17.1‰$ and $\Delta'^{17}O = -0.050‰$ formed from the weathering of igneous crust of $\delta^{18}O = 7‰$ and $\Delta'^{17}O =$ -

0.048‰ and metamorphic crust of $\delta^{18}O$ = 12‰ and $\Delta'^{17}O$ = -0.053‰ (Muehlenbachs, 1998; Bindeman et al., 2018; Sengupta and Pack, 2018). The F_{CW} estimate is large and ≈ 1/2 F_{HT} and results in the depletion of $\delta^{18}O$ and enrichment of $\Delta'^{17}O$ to the oceans.

Continental growth through sediment recycling (*CG*) results from subduction of oceanic lithosphere with a marine sediment layer with an average $\delta^{18}O$ = 26‰ and $\Delta'^{17}O$ = -0.097‰ into the mantle (Sharp et al., 2016). This model considers the subducting slab to be 90% basaltic crust and 10% ocean precipitated SiO_2 sediments with a small F_{CG} ≈ 1/12 F_{HT}. The average triple oxygen isotope composition of oceanic lithosphere was calculated using an unaltered reservoir $\delta^{18}O$ = 5.5‰ and $\Delta'^{17}O$ = -0.057‰ from Cano et al. (2020), average high and low temperature altered oceanic lithosphere $\delta^{18}O_{HT}$ = 4.4‰ and $\delta^{18}O_{LT}$ = 9.6‰ values from Muehlenbachs (1998), and corresponding altered reservoir $\Delta'^{17}O_{HT}$ = -0.050‰ and $\Delta'^{17}O_{LT}$ = -0.082‰ determined in this study. Multiplying these values by their relative proportions from the flux equations yields an estimated average basaltic crust of $\delta^{18}O$ = 5.1‰ and $\Delta'^{17}O$ = -0.052‰. The mantle is estimated to have an average $\delta^{18}O$ = 5.6‰ and $\Delta'^{17}O$ = -0.060‰ (Cano et al., 2020). $\delta^{18}O$ depletion and $\Delta'^{17}O$ enrichment of the oceans is reflected in the high $\delta^{18}O$ and low $\Delta'^{17}O$ values of island arcs compared to intraplate derived volcanic crust, which is generated through the assimilation of chemical marine sediments into the mantle.

Mantle recycling of subducted water results from the subduction of chemically bound water in the altered oceanic crust, as well as water trapped in sediment pores, that equilibrates with the mantle and is volcanically outgassed at higher $\delta^{18}O$

and lower $\Delta'^{17}O$ values. Muehlenbachs (1998) estimated a 3‰ fractionation between oceanic lithosphere and chemically bound water which can be used to estimate recycled water $\delta^{18}O$. Using a $\theta = 0.528$ between rock and water, the $\delta^{17}O$ of the water can also be estimated (Sengupta and Pack, 2018). The F_{MR} estimate is small and ≈ 1/23 F_{HT} and results in a minor enrichment of $\delta^{18}O$ and minor depletion of $\Delta'^{17}O$ to the oceans.

The steady state results of running the model can be seen in **Fig. 5**. While examining the effects large increases or decreases in the budget-dominating *HT* and *CW* processes on seawater $\delta^{18}O$ and $\Delta'^{17}O$ it was found that large increases and decreases in either flux result in no net change in seawater $\delta^{18}O$ or $\Delta'^{17}O$ because the model has reached a steady state condition. I.e., increasing F_{CW} by 100x results in the same seawater $\delta^{18}O$ and $\Delta'^{17}O$ as increasing F_{CW} by 1000x. The sensitivity of the model to changes in $\Delta'^{17}O$ values for the altered *CW* reservoir was examined to account for uncertainties in $\Delta'^{17}O$ measurements and estimates. Sensitivity tests varying the shale $\Delta'^{17}O$ = -0.050‰ by ± 0.01‰ are shown in **Fig. 6**. Using a shale with $\Delta'^{17}O$ = -0.060‰ decreases the λ from λ = 0.524 to λ = 0.523 for the decreasing F_{HT} seawater evolution and results in a maximum $\Delta'^{17}O$ = 0.019 at F_{HT} = 0, a very minor $\Delta'^{17}O$ increase from the original $\Delta'^{17}O$ = 0.014 (**Fig. 6a**). Similarly, a shale with $\Delta'^{17}O$ = -0.040‰ results in a minor increase in λ to λ=0.525 and a seawater $\Delta'^{17}O$ = 0.011 at F_{HT} = 0. Using a shale with $\Delta'^{17}O$ = -0.060‰ results in a F_{CW} increasing seawater evolution trend with λ = 0.526 and F_{CW} × 100 seawater $\Delta'^{17}O$ = 0.019, a small decrease in λ and moderate increase in seawater $\Delta'^{17}O$ from the original trend (**Fig. 6b**). A shale with $\Delta'^{17}O$ = -0.040‰ results in effectively no change in λ and

results in minor decrease in seawater $\Delta'^{17}O$ = 0.000‰ at F_{CW} × 100. Reduction of F_{MR} to a significantly lower value has been proposed by Miller et al. (2020) using seismic anisotropy measurements of the Middle America Trench. Running the model with F_{MR} from Miller et al. (2021) reduces F_{MR} by ~ 77%, effectively shutting off *MR*, and can bring the modeled seawater to a mean $\delta^{18}O$ = -0.37‰ with an unchanged $\Delta'^{17}O$ = -0.002. These calculations imply that if most bound and connate lithospheric water is discharged prior to subduction, the model comes into better agreement with the $\delta^{18}O$ ice-free estimate by only ~ -.08‰.

Using an Archean shale value of $\delta^{18}O$ = 13.052‰ and $\Delta'^{17}O$ = -0.021‰ from Bindeman et al. (2018) in the model to simulate a different Archean *CW* environment generates a modeled seawater of $\delta^{18}O$ = 0.70‰ and $\Delta'^{17}O$ = -0.011‰. This seawater $\delta^{18}O$ is heavy, but still significantly lighter than the proposed Archean seawater $\delta^{18}O$ = 3.3‰ from Johnson and Wing (2020). When F_{CW} is increased, the seawater composition evolves to a minimum $\delta^{18}O$ = -3.24‰ and $\Delta'^{17}O$ = -0.035‰, a $\delta^{18}O$ value heavier and $\Delta'^{17}O$ value significantly lighter than our standard modeled F_{HT} × 0 and F_{CW} × 100 seawater compositions. The transposed SiO_2 – H_2O equilibrium fractionation curve to this modeled F_{CW} × 100 Archean seawater composition can be seen in **Fig. 7**. This modeled seawater transposes the equilibrium fractionation curve far below most pristine Lowe et al. (2020) and Sengupta et al. (2020) samples, placing the samples in a space where diagenetic mixing models cannot account for their composition using this F_{CW} × 100 modeled seawater and transposed equilibrium fractionation curve.

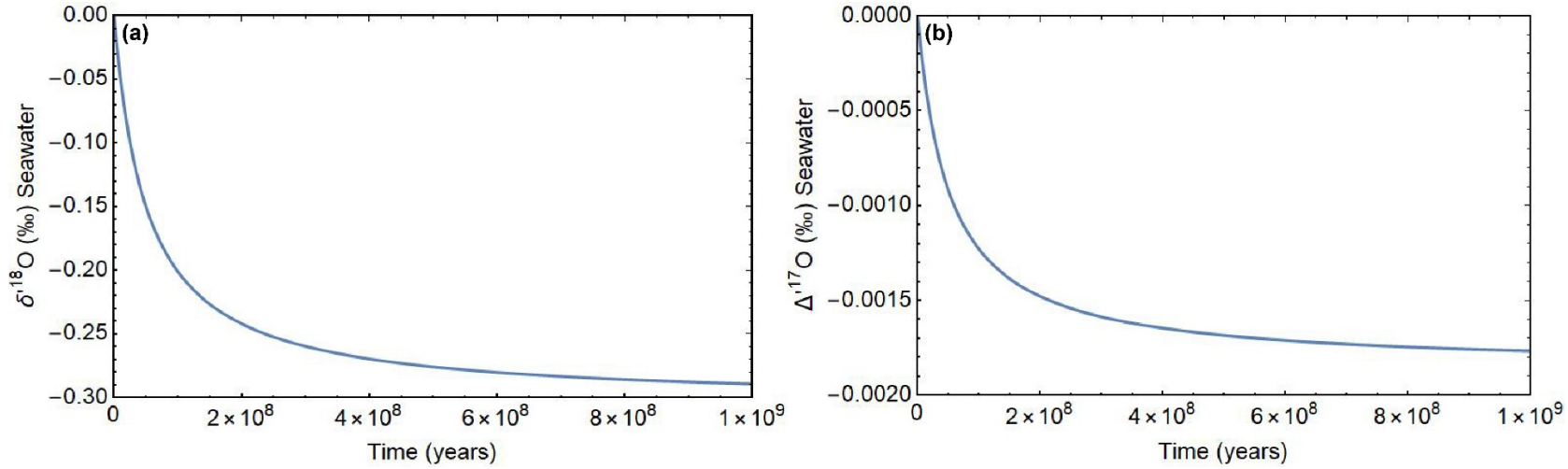

Fig. 5. Model variation in seawater $\delta^{18}O$ and $\Delta'^{17}O$ over time. (a) shows variation in seawater $\delta^{18}O$ over time. The model initially generates a seawater composition with $\delta^{18}O \approx 0‰$ and evolves to lighter values overtime with steady state reached at ~ (0.5 to 1) x 10^9 years with $\delta^{18}O \approx -0.29‰$. **(b)** shows variation in seawater $\Delta'^{17}O$ over time. The model generates a seawater $\Delta'^{17}O \approx 0.000‰$ at time zero and evolves to a lighter $\Delta'^{17}O = -0.002‰$ over ~ (0.5 to 1) x 10^9 years as steady state is reached.

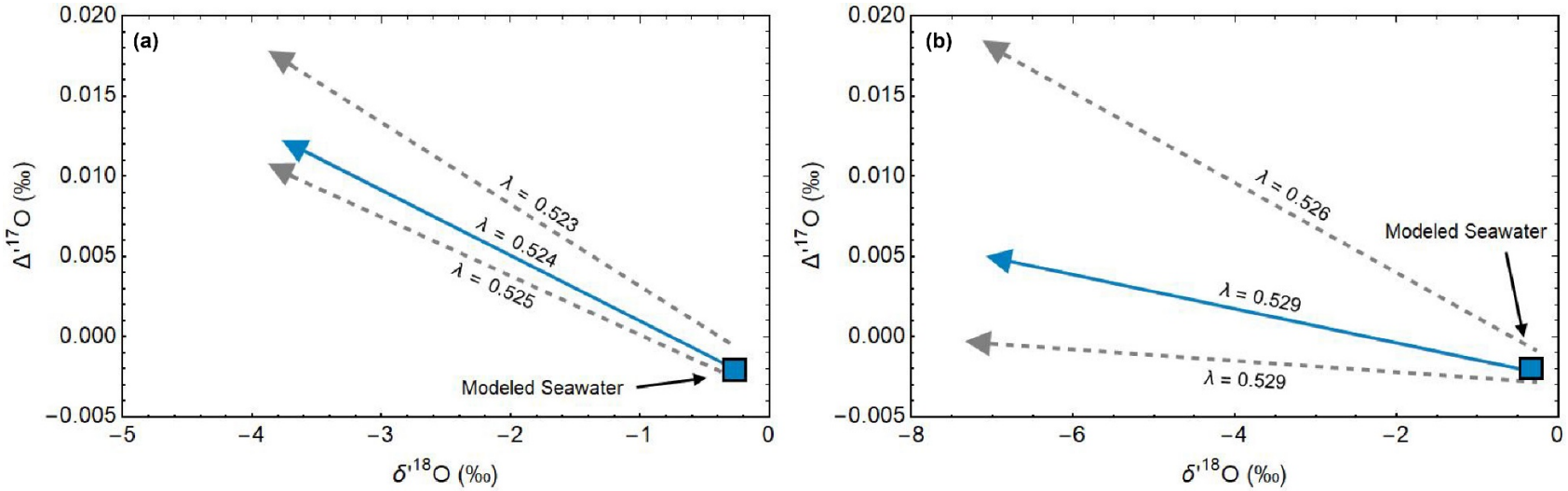

Fig. 6. Sensitivity tests of F_{HT} × 0 and F_{CW} × 100 seawater evolution trends. (a) shows changes in slope λ and seawater compositions for F_{HT} × 0 as *CW* shale endmember is varied between standard modeled $\Delta'^{17}O$ = -0.050‰ to $\Delta'^{17}O$ = -0.060‰ (λ = 0.523) and $\Delta'^{17}O$ = -0.040‰ (λ = 0.525). With λ = 0.523, seawater can evolve to a maximum $\Delta'^{17}O$ = 0.019 and with λ = 0.523 seawater evolves to a maximum $\Delta'^{17}O$ = 0.011‰. **(b)** shows changes in λ and seawater compositions for F_{CW} × 100 as the shale $\Delta'^{17}O$ varies. With λ = 0.526, seawater can evolve to a maximum $\Delta'^{17}O$ = 0.019 and with λ = 0.529 seawater can evolve to a maximum $\Delta'^{17}O$ = 0.000‰.

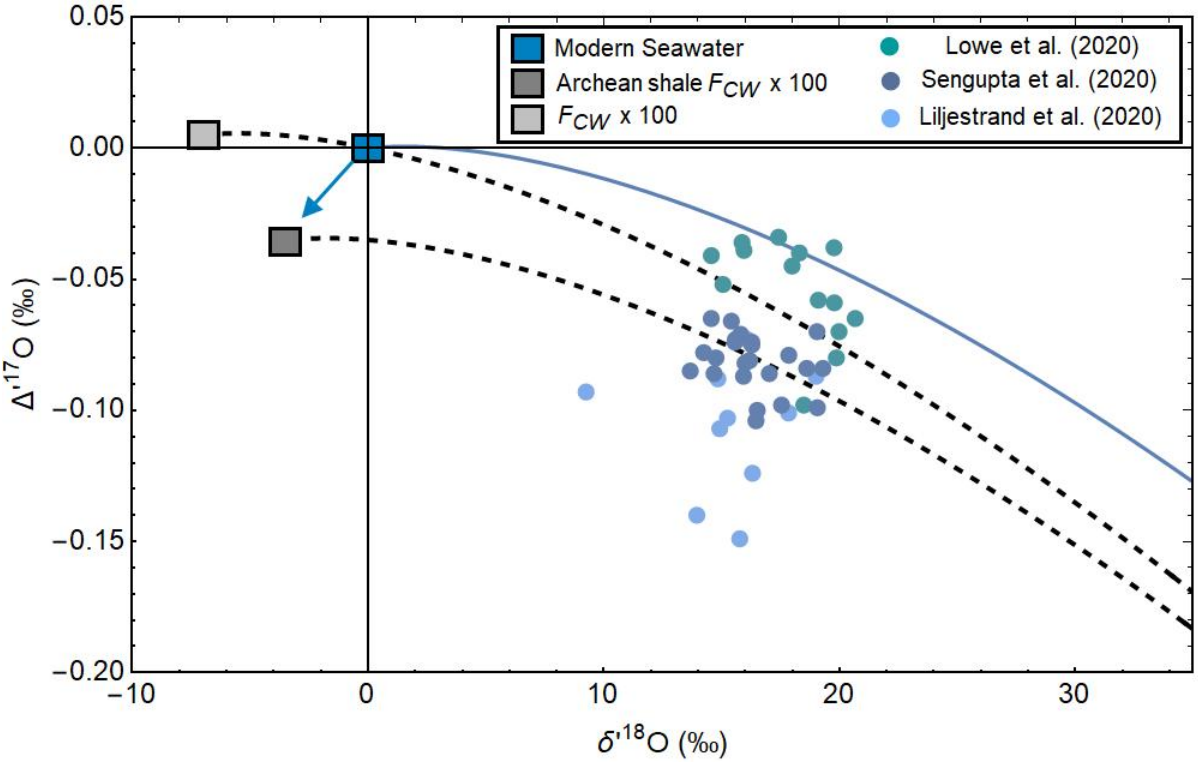

Fig. 7. Plot of modern and model generated seawater compositions with transposed SiO_2–H_2O equilibrium fractionation curves to test Archean chert equilibration using an Archean shale endmember for *CW*. When using an Archean shale of $\delta^{18}O$ = 13.052‰ and $\Delta'^{17}O$ = -0.021‰ in the *CW* Δ equations (Bindeman et al., 2018), seawater evolves to $\delta^{18}O$ = -3.24‰ and $\Delta'^{17}O$ = -0.035‰ for F_{CW} × 100. This minimum seawater composition is significantly lighter in $\Delta'^{17}O$ than any other model generated seawater and places the transposed SiO_2 – H_2O equilibrium fractionation curve below most plotted Archean cherts. Like the standard modeled F_{CW} × 100 seawater composition, this modeled seawater value cannot explain the Archean chert data with either higher ocean temperatures or diagenetic alteration and implies that secular changes in seawater composition are not the result of changes in F_{CW}.

Appendix VI: Diagenetic Alteration Modelling

Diagenetic fluid modelling was run according to the following equation after Taylor (1978):

$$\delta^{x}O_{final\ rock} = \frac{1000X + \alpha(X \times \delta^{x}O_{initial\ rock} - X \times \delta^{x}O_{initial\ water} - \delta^{x}O_{initial\ rock} - 1000X)}{\alpha X - \alpha - X} \quad (11)$$

where $\delta^{x}O$ is the delta composition for oxygen of atomic mass x, X is the F/R ratio, and α if the fractionation factor between the rock and water for ^{x}O. α values for SiO_2 – H_2O were calculated from Sharp et al. (2016) and vary for each alteration temperature. All samples from Lowe et al. (2020), Sengupta et al. (2020), and all but 3 samples from Liljestrand (2020) can be explained by a precipitation with our modeled F_{HT} × 0 seawater composition with an initial rock of $\delta^{18}O$ = 26.0‰ and $\Delta'^{17}O$ = -0.096‰, corresponding to an ocean temperature of 50°C (Lowe et al., 2020). Fluids with compositions ranging from $\delta^{18}O$ = -7 to -20‰ and $\Delta'^{17}O$ = 0.03 to 0.04‰ and alteration temperatures ranging from 50 to 200°C are required to explain the chert compositions. Samples from Liljestrand et al. (2020) generally require lighter $\delta^{18}O$ fluids and higher alteration temperatures than Lowe et al. (2020) and Sengupta et al. (2020), likely due to a higher degree of diagenetic alteration as suggested by Lowe et al. (2020). It is important to recognize that in nearly all samples, a calculated F/R ratio using a given alteration temperature and fluid composition is not unique and multiple solutions exist to account for each sample $\delta^{18}O$ and $\Delta'^{17}O$ value. For a given sample suite, the solution alteration temperatures and diagenetic fluid composition that best fits the data is typically used. In **Fig. 4**, each study presents data from different sample suites and in the cases of Sengupta et al. (2020) and Liljestrand et al. (2020) there are multiple sample suites within the

data set and finding a best fit for fluid composition and alteration temperature that matches all data presented is unattainable.

References

Alt, J. C. *et al.* Hydrothermal alteration of a section of upper oceanic crust in the Eastern equatorial pacific: A synthesis of results from site 504 (DSDP legs 69, 70, and 83, and ODP legs 111, 137, 140, and 148). in *Proceedings of the Ocean Drilling Program, 148 Scientific Results* (Ocean Drilling Program, 1996).

Alt, J. C., Laverne, C. & Muehlenbachs, K. Alteration of the upper oceanic crust: Mineralogy and processes in deep sea drilling project hole 504B, leg 83. in *Initial Reports of the Deep Sea Drilling Project* (U.S. Government Printing Office, 1985).

Alt, J. C., Muehlenbachs, K. & Honnorez, J. An oxygen isotopic profile through the upper kilometer of the oceanic crust, DSDP Hole 504B. *Earth Planet. Sci. Lett.* **80**, 217–229 (1986).

Banner, J. L. & Hanson, G. N. Calculation of simultaneous isotopic and trace element variations during water-rock interaction with applications to carbonate diagenesis. *Geochim. Cosmochim. Acta* **54**, 3123–3137 (1990).

Bindeman, I. N. *et al.* Rapid emergence of subaerial landmasses and onset of a modern hydrologic cycle 2.5 billion years ago. *Nature* **557**, 545–548 (2018).

Cano, E. J., Sharp, Z. D. & Shearer, C. K. Distinct oxygen isotope compositions of the Earth and Moon. *Nat. Geosci.* **13**, 270–274 (2020).

Carpenter, S. J. *et al.* $\delta^{18}O$ values, and Sr/Mg ratios of Late Devonian abiotic marine calcite: Implications for the composition of ancient seawater. *Geochim. Cosmochim. Acta* **55**, 1991–2010 (1991).

Clayton, R. N. & Mayeda, T. K. The use of bromine pentafluoride in the extraction of oxygen from oxides and silicates for isotopic analysis. *Geochim. Cosmochim. Acta* **27**, 43–52 (1963).

Cole, D. R., Mottl, M. J. & Ohmoto, H. Isotopic exchange in mineral-fluid systems. II. Oxygen and hydrogen isotopic investigation of the experimental basalt-seawater system. *Geochim. Cosmochim. Acta* **51**, 1523–1538 (1987).

Coogan, L. A. & Dosso, S. E. Alteration of ocean crust provides a strong temperature dependent feedback on the geological carbon cycle and is a primary driver of the Sr-isotopic composition of seawater. *Earth Planet. Sci. Lett.* **415**, 38–46 (2015).

Coogan, L. A. & Gillis, K. M. Evidence that low-temperature oceanic hydrothermal systems play an important role in the silicate-carbonate weathering cycle and long-term climate regulation: OCEANIC HYDROTHERMAL CARBONATE UPTAKE. *Geochem. Geophys. Geosyst.* **14**, 1771–1786 (2013).

Craig, H. Isotopic standards for carbon and oxygen and correction factors for mass-spectrometric analysis of carbon dioxide. *Geochim. Cosmochim. Acta* **12**, 133–149 (1957).

Garcia, A. K., Schopf, J. W., Yokobori, S.-I., Akanuma, S. & Yamagishi, A. Reconstructed ancestral enzymes suggest long-term cooling of Earth's photic zone since the Archean. *Proc. Natl. Acad. Sci. U. S. A.* **114**, 4619–4624 (2017).

Gillis, K. M., Snow, J.E., Klaus, A., Guerin, G., Abe, N., Akizawa, N., Ceuleneer, G., Cheadle, M.J., Adriao, A., Faak, K., Falloon, T.J., Friedman, S.A., Godard, M.M., Harigane, Y., Horst, A.J., Hoshide, T., Ildefonse, B., Jean, M.M., John, B.E., Koepke, J.H., Machi, S., Maeda, J., Marks, N.E., McCaig, A.M., Meyer, R., Morris, A., Nozaka, T., Python, M., Saha, A., Wintsch, R.P. Hole U1415AJ. in *Proceedings of the IODP* (Integrated Ocean Drilling Program, 2014).

Jaffrés, J. B. D., Shields, G. A. & Wallmann, K. The oxygen isotope evolution of seawater: A critical review of a long-standing controversy and an improved geological water cycle model for the past 3.4 billion years. *Earth Sci. Rev.* **83**, 83–122 (2007).

Johnson, B. W. & Wing, B. A. Limited Archaean continental emergence reflected in an early Archaean ^{18}O-enriched ocean. *Nat. Geosci.* **13**, 243–248 (2020).

Karhu, J. & Epstein, S. The implication of the oxygen isotope records in coexisting cherts and phosphates. *Geochim. Cosmochim. Acta* **50**, 1745–1756 (1986).

Kasting, J. F. *et al.* Paleoclimates, ocean depth, and the oxygen isotopic composition of seawater. *Geochim. Cosmochim. Acta* **70**, A307 (2006).

Knauth, L. P. & Epstein, S. Hydrogen and oxygen isotope ratios in nodular and bedded cherts. *Geochim. Cosmochim. Acta* **40**, 1095–1108 (1976).

Knauth, L. P. & Lowe, D. R. Oxygen isotope geochemistry of cherts from the Onverwacht Group (3.4 billion years), Transvaal, South Africa, with implications for secular variations in the isotopic composition of cherts. *Earth Planet. Sci. Lett.* **41**, 209–222 (1978).

Levin, N. E., Raub, T. D., Dauphas, N. & Eiler, J. M. Triple oxygen isotope variations in sedimentary rocks. *Geochim. Cosmochim. Acta* **139**, 173–189 (2014).

Liljestrand, F. L. *et al.* The triple oxygen isotope composition of Precambrian chert. *Earth Planet. Sci. Lett.* **537**, 116167 (2020).

Lowe, D. R., Ibarra, D. E., Drabon, N. & Chamberlain, C. P. Constraints on surface temperature 3.4 billion years ago based on triple oxygen isotopes of cherts from the Barberton Greenstone Belt, South Africa, and the problem of sample selection. *Am. J. Sci.* **320**, 790–814 (2020).

Luz, B. & Barkan, E. Variations of $^{17}O/^{16}O$ and $^{18}O/^{16}O$ in meteoric waters. *Geochim. Cosmochim. Acta* **74**, 6276–6286 (2010).

McKinney, C. R., McCrea, J. M., Epstein, S., Allen, H. A. & Urey, H. C. Improvements in mass spectrometers for the measurement of small differences in isotope abundance ratios. *Rev. Sci. Instrum.* **21**, 724–730 (1950).

Miller, N. C., Lizarralde, D., Collins, J. A., Holbrook, W. S. & Van Avendonk, H. J. A. Limited mantle hydration by bending faults at the middle America trench. *J. Geophys. Res. Solid Earth* **126**, (2021).

Muehlenbachs, K. & Clayton, R. N. Oxygen isotope composition of the oceanic crust and its bearing on seawater. *J. Geophys. Res.* **81**, 4365–4369 (1976).

Muehlenbachs, K. & Clayton, R. N. Oxygen isotope geochemistry of submarine greenstones. *Can. J. Earth Sci.* **9**, 471–478 (1972).

Muehlenbachs, K. The alteration and aging of the basaltic layer of sea floor: Oxygen isotope evidence from DSDP/IPOD legs 51, 52, and 53. in *Initial Reports of the Deep Sea Drilling Project* (U.S. Government Printing Office, 1980).

Pack, A. & Herwartz, D. The triple oxygen isotope composition of the Earth mantle and understanding $\Delta^{17}O$ variations in terrestrial rocks and minerals. *Earth Planet. Sci. Lett.* **390**, 138–145 (2014).

Perry, E. C., Jr. The oxygen isotope chemistry of ancient cherts. *Earth Planet. Sci. Lett.* **3**, 62–66 (1967).

Sengupta, S. & Pack, A. Triple oxygen isotope mass balance for the Earth's oceans with application to Archean cherts. *Chem. Geol.* **495**, 18–26 (2018).

Sengupta, S., Peters, S. T. M., Reitner, J., Duda, J.-P. & Pack, A. Triple oxygen isotopes of cherts through time. *Chem. Geol.* **554**, 119789 (2020).

Shackleton, N. J. & Kennett, J. P. Paleotemperature history of the Cenozoic and the initiation of antarctic glaciation: Oxygen and carbon isotope analyses in DSDP sites 277, 279 and 281. in *Initial Reports of the Deep Sea Drilling Project* (U.S. Government Printing Office, 1975).

Sharp, Z. D. A laser-based microanalytical method for the in situ determination of oxygen isotope ratios of silicates and oxides. *Geochim. Cosmochim. Acta* **54**, 1353–1357 (1990).

Sharp, Z. D. *et al.* A calibration of the triple oxygen isotope fractionation in the SiO2–H2O system and applications to natural samples. *Geochim. Cosmochim. Acta* **186**, 105–119 (2016).

Sharp, Z. D., Wostbrock, J. A. G., Pack, A. Mass-dependent triple oxygen isotope variations in terrestrial materials. *Geochem. perspect. lett.* 27–31 (2018).

Schauble, E., Young, E. Mass Dependence of Equilibrium Oxygen Isotope Fractionation in Carbonate, Nitrate, Oxide, Perchlorate, Phosphate, Silicate, and Sulfate Minerals. *Reviews in Mineralogy and Geochemistry*, **86**, pp.137-178 (2021).

Shields, G. A. Chapter 7.6 the marine carbonate and chert isotope records and their implications for tectonics, life and climate on the early earth. in *Earth's Oldest Rocks* 971–983 (Elsevier, 2007).

Tartèse, R., Chaussidon, M., Gurenko, A., Delarue, F. & Robert, F. Warm Archaean oceans reconstructed from oxygen isotope composition of early-life remnants. *Geochem. perspect. lett.* 55–65 (2017).

Taylor, H. P. & Epstein, S. Relationship between O^{18}/O^{16} ratios in coexisting minerals of igneous and metamorphic rocks. *Geol. Soc. Am. Bull.* **73**, 675 (1962).

Taylor, H. P., Jr. Oxygen and hydrogen isotope studies of plutonic granitic rocks. *Earth Planet. Sci. Lett.* **38**, 177–210 (1978).

Veizer, J. *et al.* $^{87}Sr/^{86}Sr$, $\delta^{13}C$ and $\delta^{18}O$ evolution of Phanerozoic seawater. *Chem. Geol.* **161**, 59–88 (1999).

Walker, J. C. G. & Lohmann, K. C. Why the oxygen isotopic composition of sea water changes with time. *Geophys. Res. Lett.* **16**, 323–326 (1989).

Wallmann, K. The geological water cycle and the evolution of marine $\delta^{18}O$ values. *Geochim. Cosmochim. Acta* **65**, 2469–2485 (2001).

Weber, J. N. Evolution of the oceans and the origin of fine-grained dolomites. *Nature* **207**, 930–933 (1965).

Wenzel, B., Lécuyer, C. & Joachimski, M. M. Comparing oxygen isotope records of silurian calcite and phosphate—$\delta^{18}O$ compositions of brachiopods and conodonts. *Geochim. Cosmochim. Acta* **64**, 1859–1872 (2000).

Wostbrock, J. A. G., Cano, E. J. & Sharp, Z. D. An internally consistent triple oxygen isotope calibration of standards for silicates, carbonates and air relative to VSMOW2 and SLAP2. *Chem. Geol.* **533**, 119432 (2020).

Sharp, Z. D., Wostbrock, J. A. Standardization for the Triple oxygen Isotope system: Waters, Silicates, Carbonates, air, and sulfates. Reviews in Mineralogy and Geochemistry, **86**,179-196 (2021).

Zakharov, D. O. & Bindeman, I. N. Triple oxygen and hydrogen isotopic study of hydrothermally altered rocks from the 2.43–2.41 Ga Vetreny belt, Russia: An insight into the early Paleoproterozoic seawater. *Geochim. Cosmochim. Acta* **248**, 185–209 (2019).